# Multinuclear, Multifield, and Multiphase Nuclear Magnetic Resonance Study of Cadmium *meso*-Tetraphenylporphyrin and Its Pyridine Adduct

**Hans J. Jakobsen,*[1a] Paul D. Ellis,*[1b] Ruth R. Inners,[1b] and Claus F. Jensen[1a]**

*Contribution from the Departments of Chemistry, University of Aarhus, 8000 Aarhus C, Denmark, and the University of South Carolina, Columbia, South Carolina 29208.*
*Received February 10, 1982*

**Abstract:** Multifield $^{113}Cd$, $^{15}N$, and $^{13}C$ NMR spectra at 2.3, 4.7, and 9.4 T have been obtained for the pyridine adduct of $^{113}Cd$ and $^{15}N$ multiplylabeled cadmium *meso*-tetraphenylporphyrin (Py–Cd–TPP). The chemical shifts, signs, and magnitudes of spin–spin coupling constants and spin–lattice relaxation parameters/mechanisms for these nuclei have been determined in solution. The sign of the $^{113}Cd$–$^{15}N$ coupling constant is found to be positive, $^1J(^{113}Cd–^{15}N) = +150.1$ Hz. Further, solid-state $^{113}Cd$ NMR experiments (with and without magic angle spinning) have been performed for Py–Cd–TPP and "unliganded" Cd–TPP. The latter data have been used for an evaluation of the origin of the $^{113}Cd$ relaxation data for Py–Cd–TPP in solution. From these data, a 33-ppm $^{113}Cd$ chemical shift to lower shielding is observed upon adduct formation, i.e., on going from Cd–TPP to Py–Cd–TPP. This chemical shift is attributable to the donor properties of the fifth (pyridine) ligand plus its effect of pulling the cadmium out of the porphyrin ring. The chemical shift anisotropies for the axially symmetric $^{113}Cd$ shielding tensors, $\Delta\sigma = \sigma_{\parallel} - \sigma_{\perp}$, are $-341 \pm 3$ and $-105 \pm 2$ ppm for Cd–TPP and Py–Cd–TPP, respectively. Appropriate equations required for the analysis of relaxation data in terms of the anisotropic rotational diffusion for Py–Cd–TPP and librational motion of the phenyl-group substituents have been derived. From a combination of liquid- and solid-state data, the anisotropy in the molecular motion for Py–Cd–TPP in solution has been determined to be $D_{\parallel}/D_{\perp} = 3.2 \pm 0.8$. Finally, the diffusion constant for the librational rotational motion of the phenyl-group substituents relative to the porphysin-ring skeleton is determined to be $D^* = (2.2 \pm 0.8) \times 10^9$ s$^{-1}$.

## Introduction

Metalloporphyrins[2] constitute the prosthetic group in a number of important proteins. Furthermore, the biochemically significant functions of these metalloproteins are controlled by their central metals, coordinating axial ligands, and protein environment and by the interaction between the central metal and the porphyrin nitrogens. Thus, iron porphyrin proteins are involved in fundamental processes such as respiration (hemoglobin and myoglobin)[3] and electron transport (cytochromes)[4] whereas magnesium compounds derived from di- and tetrahydroporphyrins, pheophytins, and chlorophylls are involved in the photosynthesis reactions in algae, bacteria, and green plants.[5,6]

Over the past several years, $^{113}Cd$ NMR spectroscopy[7] has become a valuable tool in inorganic and bioinorganic chemistry. The utility of cadmium arises because of two factors, the relative ease of performing $^{113}Cd$ NMR experiments and the ability of cadmium to replace calcium and zinc in biological systems while retaining activity (albeit altered). Cadmium-113 NMR spectroscopy has been employed to study cadmium in both solutions (aqueous,[7,8] supercooled aqueous,[9] and nonaqueous[7,10]) and the solid state,[11] organocadmium compounds,[7a,c] and cadmium-substituted metalloproteins.[12] The $^{113}Cd$ chemical shift range observed in these studies spans in excess of 800 ppm and thus provides an excellent tool to probe subtle differences in the local environment for cadmium. In order to refine our knowledge of the relationship between $^{113}Cd$ NMR parameters (shielding constants, coupling constants, and relaxation times) and molecular structure and motion, we have initiated investigations of these parameters for selected compounds in both the liquid and solid phase.

With this objective in mind, cadmium-substituted porphyrins represent an intriguing series of compounds since potentially they allow studies of cadmium in a novel bonding environment. Further, one can envision perturbing this environment by the addition of a variety of Lewis bases to probe the effects of forming five or six coordinated species.[13] The results of the latter studies would have direct bearing upon the possibility of employing $^{113}Cd$ FT NMR methods as a means of investigating cadmium-substituted myoglobins and hemoglobins.

(1) (a) University of Aarhus; (b) University of South Carolina.
(2) K. M. Smith, Ed., "Porphyrins and Metalloporphyrins", Elsevier, Amsterdam, 1975.
(3) E. Antonini and M. Burnori, "Hemoglobin and Myoglobin in Their Reactions with Ligands", Elsevier, New York, in press.
(4) R. Lemberg and J. Barrett, "Cytochrome", Academic Press, New York, 1973.
(5) L. D. Vernon and G. R. Seely, Eds., "The Chlorophylls", Academic Press, New York, 1966.
(6) R. K. Clayton and W. R. Sistrom, Eds., "The Photosynthetic Bacteria", Plenum Press, New York, 1978.
(7) (a) G. E. Maciel and M. Borzo, *J. Chem. Soc., Chem. Commun.*, 394 (1973); (b) R. J. Kostelnik and A. A. Bothner-By, *J. Magn. Reson.*, **14**, 141 (1974); (c) A. D. Cardin, P. D. Ellis, J. D. Odom, and J. W. Howard, Jr., *J. Am. Chem. Soc.*, **97**, 1672 (1975).
(8) C. F. Jensen, S. Deshmukh, H. J. Jakobsen, R. R. Inners, and P. D. Ellis, *J. Am. Chem. Soc.*, **103**, 3659 (1981), and references cited herein.
(9) (a) M. J. B. Ackerman and J. J. H. Ackerman, *J. Phys. Chem.*, **84**, 3151 (1980); (b) H. J. Jakobsen and P. D. Ellis, *ibid.*, **85**, 3367 (1981).
(10) (a) T. Maitani and K. T. Suzuki, *Inorg. Nucl. Chem. Lett.* **15**, 213 (1979); (b) R. Colton and D. Dakternieks, *Aust. J. Chem.* **33**, 1677 (1980); (c) R. Colton and D. Dakternieks, *ibid.*, **33**, 2405 (1980).
(11) (a) J. J. Ackerman, T. V. Orr, V. J. Bartuska, and G. E. Maciel, *J. Am. Chem. Soc.*, **101**, 341 (1979); (b) P. G. Mennitt, M. P. Shatlock, V. J. Bartuska, and G. E. Maciel, *J. Phys. Chem.*, **85**, 2087 (1981). (c) T. T. P. Cheung, L. E. Worthington, L. E. Murphy, P. DuPois Murphy, and B. C. Gerstein, *J. Magn. Reson.*, **41**, 158 (1980); (d) P. DuPois Murphy and B. C. Gerstein, *J. Am. Chem. Soc.*, **103**, 3282 (1981); (e) P. DuBois Murphy, W. C. Stevens, T. T. P. Cheung, S. Lacelle, B. C. Gerstein, and D. M. Kurtz, Jr., *ibid.*, **103**, 4400 (1981).
(12) For a collection of references prior to 1980 see ref 8. (a) S. Forsén, E. Thullin, T. Drakenberg, J. Krebs, and K. Seamon, *FEBS Lett.* **177**, 189 (1980), (b) B. R. Robsein and R. J. Myers, *J. Am. Chem. Soc.*, **102**, 2453 (1980); (c) D. B. Bailey, P. D. Ellis, and J. A. Fee, *Biochemistry*, **19**, 591 (1980); (d) A. R. Palmer, D. B. Bailey, A. D. Cardin, P. P. Yang, W. D. Behnke, and P. D. Ellis, *ibid.*, **19**, 4031 (1980); (e) J. D. Otvos and I. M. Armitage, *ibid.*, **19**, 4031 (1980); (f) A. J. M. S. Uiterkamp, I. M. Armitage, and J. E. Coleman, *J. Biol. Chem.*, **255**, 3911 (1980); (g) B. R. Robsein and R. J. Myers, *ibid.*, **256**, 5313 (1981); (h) J. D. Otvos and I. M. Armitage, *Proc. Natl. Acad. Sci., U.S.A.*, **77**, 7094 (1980); (i) N. B. H. Jonsson, L. A. E. Tibell, J. Evelhoch, S. J. Bell, and J. L. Sudmeier, *ibid.*, **77**, 3269 (1980); (j) J. L. Sudmeier, S. J. Bell, M. C. Strom, and M. F. Dunn, *Science*, **212**, 560 (1981); (k) J. L. Evelhoch, D. F. Bocian, and J. L. Sudmeier, *Biochemistry*, **20**, 4951 (1981).
(13) (a) C. H. Kirksey and P. Hambright, *Inorg. Chem.*, **9**, 958 (1970); (b) P. F. Rodesiler, E. H. Griffith, P. D. Ellis, and E. L. Amma, *J. Chem. Soc., Chem. Commun.*, **492** (1980).

0002-7863/82/1504-7442$01.25/0 

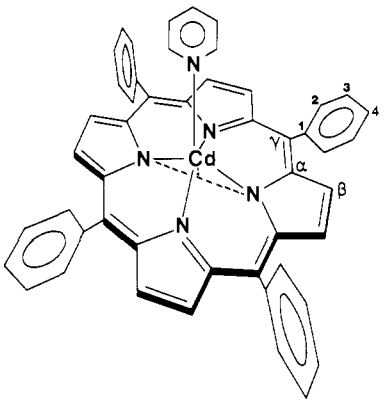


Figure 1. Structural formula of the pyridine adduct of cadmium *meso*-tetraphenylporphyrin, Py-Cd-TPP (**1**).

Metalloporphyrins have been extensively studied by virtually every conceivable spectroscopic technique. From the perspective of high-resolution NMR spectroscopy, $^1H$ and $^{13}C$ NMR have been utilized to the highest degree.[14] More recently $^{15}N$ NMR employing $^{15}N$-enriched samples has met with moderate success.[15] From the point of view of studying the consequences of axial ligand binding to metal, it seems prudent to examine the spectroscopy of the metal center directly. The first study with this objective in mind was performed by Yeh and co-workers.[14f] This was accomplished by studying the effects of 4-substituted pyridines on the $^{111}Cd$ chemical shift as obtained by INDOR experiments. Of the several methods which are applicable (Mössbauer, EXAFS, NMR spectroscopy, X-ray diffraction) NMR spectroscopy appears to be the method of greatest potential. However, it is equally clear that X-ray crystallography is needed to generate the critical structure/shift benchmarks. Within the boundary conditions imposed by a high-resolution metal NMR experiment, the only allowed metals are those with nuclear spin-$^1/_2$ isotopes, i.e., $^{57}Fe$, $^{113}Cd$, $^{195}Pt$, $^{199}Hg$, and $^{207}Pb$.

We are presently concerned with an investigation of the utility of liquid- and solid-state (powder and magic angle spinning) $^{113}Cd$ NMR as a vehicle in probing ligand binding to cadmium-substituted porphyrins. However, before this topic can be extensively examined, we have addressed ourselves to studying several fundamental points using cadmium *meso*-tetraphenylporphyrin, Cd-TPP, as a model system (Figure 1). These include $^{113}Cd$, $^{15}N$, and $^{13}C$ spin-lattice relaxation times/mechanisms, the relative importance of the $^{113}Cd$-$^1H$ and $^{15}N$-$^1H$ dipole-dipole relaxation mechanisms (because of the negative $\gamma$ values for $^{113}Cd$ and $^{15}N$ and resulting partial negative nuclear Overhauser effects, NOE), the anisotropy in the motion of the system in solution as monitored by liquid- and solid-state NMR techniques, $^{113}Cd$ chemical shift anisotropies, magnitudes and signs of scalar coupling constants, and the possible problem of broadening the $^{113}Cd$ resonance by $^{14}N$ scalar coupling. These aspects have been investigated in the present work which, to our knowledge, represents the first detailed investigation employing metal NMR to metalloporphyrins. A preliminary account on part of the work has recently appeared.[16]

## Experimental Section

**Materials.** The preparation of cadmium(II) *meso*-tetraphenyporphyrin (Cd-TPP) and $^{113}Cd$ and $^{15}N$ multiplylabeled Cd-TPP followed the general synthetic scheme outlined elsewhere for metalloporphyrins[17] and is given here for $^{113}Cd$-[$^{15}N_4$]TPP. Pure [$^{15}N_4$]$H_2$TPP was obtained by reaction of benzaldehyde (1.56 g) with pyrrole-$^{15}N$ (1.00 g, 96% $^{15}N$ isotope enrichment) in refluxing propionic acid; the unavoidable contamination of *meso*-tetraphenylchlorin-$^{15}N_4$ (up to 5%) was removed by treatment with 2,3-dichloro-5,6-dicyanobenzoquinone.[17a] The overall yield of pure [$^{15}N_4$]$H_2$TPP was 477 mg (21%). $^{113}CdO$ (50 mg, 96% $^{113}Cd$ isotope enrichment from Oak Ridge National Laboratory, Oak Ridge TN) was converted quantitatively to $^{113}Cd(OCOCH_3)_2$ by dissolving in glacial acetic acid (3 mL) followed by lyophylization. $^{113}Cd$-[$^{15}N_4$]TPP was obtained in quantitative yield by refluxing equimolar quantities of [$^{15}N_4$]$H_2$TPP and $^{113}Cd(OCOCH_3)_2$ in dry DMF for 30 min. Isolation of the product was accomplished by concentration of the reaction mixture followed by dilution of methanol. Pure unliganded $^{113}Cd$-[$^{15}N_4$]TPP (without solvents (DMF/methanol) attached to cadmium) was obtained as violet crystals after drying overnight in a "drying pistol" at 180 °C (refluxing *o*-dichlorobenzene) and 0.1 mmHg. Based on the 96% $^{15}N$ isotope enrichment for the pyrrole-$^{15}N$ the following composition of the $^{113}Cd$ and $^{15}N$ multiply labeled Cd-TPP has been calculated: $^{113}Cd$-[$^{15}N_4$]TPP, 81%; $^{113}Cd$-[$^{15}N_3$,$^{14}N$]TPP, 17%; $^{113}Cd$-[$^{15}N_2$,$^{14}N_2$]TPP, 1%; $^{113}Cd$-[$^{15}N$,$^{14}N_3$]TPP, 0.05%; $^{113}Cd$-[$^{14}N_4$]TPP, 0%.

For the purpose of the solid-state $^{113}Cd$ NMR studies the 1:1 adduct[13] of $^{113}Cd$-[$^{15}N_4$]TPP and pyridine-$^{15}N$ (95% $^{15}N$ isotope enrichment) was isolated. This was achieved by dissolving unliganded $^{113}Cd$-[$^{15}N_4$]TPP in a solution of $CDCl_3$ containing a 5 M excess of pyridine-$^{15}N$. The solvent and excess ligand were allowed to evaporate at room temperature and standard pressure leaving violet crystals of the 1:1 adduct [$^{15}N$]-Py—$^{113}Cd$-[$^{15}N_4$]TPP.

The Cd-TPP concentration of the NMR sample solutions was 0.023 M and all solutions were prepared by using $CDCl_3$ as solvent and pyridine or pyridine-$d_5$ as the axial ligand for the formation of the 1:1 Py—Cd-TPP complex.[13] The pyridine ligand was present in a 10 M excess in all samples. It should be noted that pure unliganded Cd-TPP shows pronounced aggregation and is almost insoluble in $CDCl_3$ alone.[14b] However, addition of a donor molecule such as pyridine dissociates any aggregates and dramatically increases the solubility. The solutions were contained in 10-mm NMR sample tubes for most of the experiments performed; however, 18-mm tubes were used for the low-field (XL-100) $^{15}N$ NMR studies.

**NMR Spectra.** Solution-state NMR spectra were recorded at three different magnetic field strengths; 2.3, 4.7, and 9.4 T. $^{113}Cd$ NMR spectra were recorded at all three magnetic field strengths corresponding to $^{113}Cd$ resonance frequencies of 22.19, 44.40, and 88.78 MHz, respectively. $^{15}N$ NMR spectra were recorded at 2.3 and 9.4 T corresponding to $^{15}N$ resonance frequencies of 10.14 and 40.55 MHz. $^{13}C$ NMR spectra were recorded at 9.4 T corresponding to a $^{13}C$ resonance frequency of 100.62 MHz.

Spectra at 2.3 T were obtained on a Varian XL-100-15 spectrometer, extensively modified for multinuclear NMR operation, and at a temperature of 30 °C. A locally designed high-performance 18-mm probe system described recently[18] was used with this spectrometer. $^{15}N$ spin-lattice relaxation time measurements were performed on this system using gated $^1H$ decoupling with 0.6 W of decoupling power and 100-Hz square wave modulation. Because of the long $T_1(^{15}N)$ values (ca. 90–100 s) at 2.3 T and the negative $\gamma$ value for $^{15}N$ and resulting partial negative NOE observed at 2.3 T, the $T_1(^{15}N)$ experiments were performed by using the fast inversion-recovery FT (FIRFT) method[19] with a recycle time of $2T_1$ and with the decoupler on only during acquisition of data. A set of 7 $\tau$ values was used for each $T_1(^{15}N)$ determination requiring approximately 70 h of instrument time per $T_1(^{15}N)$ experiment. The errors in $T_1(^{15}N)$ determined at this magnetic field are in the range of 5–10%. $^{15}N$-{$^1H$} NOE determinations were obtained from integrated intensities of the $^{15}N$ spectra recorded in the presence of continuous $^1H$ decoupling (0.6 W) and in the absence of decoupling. The integrated intensities were measured from expanded spectra by means of a planim-

(14) For a collection of references see Chapter 10 in ref 2. (a) R. J. Abraham, G. E. Hawkes, M. F. Hudson, and K. M. Smith, *J. Chem. Soc., Perkin Trans 2*, 204 (1975); (b) R. J. Abraham, H. Pearson, and K. M. Smith, *J. Am. Chem. Soc.*, **98**, 1604 (1976); (c) R. J. Abraham, F. Eivazi, R. Mayyir-Mazhir, H. Pearson, and K. M. Smith, *Org. Magn. Reson.*, **11**, 52 (1978); (d) J. Mispelter, M. Momenteau, and J. M. Lhoste, *J. Chem. Soc., Chem. Commun.*, 808 (1979); (e) M. a. Phillippi and H. M. Goff, *ibid.*, 455 (1980); (f) D. D. Dominguez, M. M. King, and H. J. C. Yeh, *J. Magn. Reson.*, **32**, 161 (1978).

(15) (a) S. G. Boxer, G. L. Closs, and J. J. Katz, *J. Am. Chem. Soc.*, **96**, 7058 (1974); (b) A. Lapidot, C. S. Irving, and Z. Malik, *ibid.*, **98**, 632 (1976); (c) D. Gust, R. B. Moon, and J. D. Roberts, *Proc. Natl. Acad. Sci. U.S.A.*, **72**, 4696 (1975); (d) D. Gust and J. D. Roberts, *J. Am. Chem. Soc.*, **99**, 3637 (1977); (e) K. Kawano, Y. Ozaki, Y. Kyogoku, H. Ogoshi, H. Sugimoto, and Z.-I. Yoshida, *J. Chem. Soc., Chem. Commun.*, 226 (1977); (f) I. Morishima, T. Inubushi, and M. Sato, *ibid.*, 106 (1978); (g) K. Kawano, Y. Ozaki, Y. Kyogoku, H. Sugimoto, Z.-I. Yoshida, *J. Chem. Soc., Perkin Trans. 2*, 1319 (1978); (h) D. Gust and D. N. Neal, *J. Chem. Soc., Chem. Commun.*, 681 (1978); (i) E. V. Goldammer, *Z. Naturforsch. C*, **34**, 11–6 (1979).

(16) P. D. Ellis, R. R. Inners, and H. J. Jakobsen, *J. Phys. Chem.*, **86**, 1506 (1982).

(17) (a) Reference 2, pp 769–70; (b) A. D. Adler, F. R. Longo, F. Kampas, and J. Kim, *J. Inorg. Nucl. Chem.*, **32**, 2443 (1970).

(18) P. Daugaard, P. D. Ellis, and H. J. Jakobsen *J. Magn. Reson.*, **43**, 434 (1981).

(19) D. Canet, G. C. Levy, and I. R. Peat, *J. Magn. Reson.*, **18**, 199 (1975).

eter. The sign of the $^{113}Cd-^{15}N$ coupling constant was determined from $^{15}N-\{H\}$ selective population transfer (SPT) experiments[20] which were performed as described elsewhere.[21]

Spectra at 4.7 and 9.4 T were obtained on Bruker WP-200 and WH-400 spectrometers, respectively. Spin–lattice relaxation measurements at 9.4 T were performed by using the methods of (i) inversion-recovery FT (IRFT) for $T_1(^{113}Cd)$, $T_1(^{15}N)$, and $T_1(^{13}C)$, (ii) fast inversion-recovery FT (FIRFT)[19] for $T_1(^{113}Cd)$, and (iii) saturation-recovery (SR) via CRAPS (computer rotated and alternated phase sequence)[22] for $T_1(^{113}Cd)$. Because both the $^{113}Cd-\{^1H\}$ and $^{15}N-\{^1H\}$ NOE's are very small at this magnetic field strength, continuous $^1H$ decoupling (0.6 W) was employed for all $T_1$ measurements. The number of $\tau$ values in these experiments varied from 11 to 18. Because of the increase in the value of $T_1(^{113}Cd)$ and $^{113}Cd-\{^1H\}$ NOE values at 4.7 T, the $T_1(^{113}Cd)$ measurements at 44.40 MHz were performed by the SR (CRAPS) method only with gated $^1H$ decoupling (decoupler on only during acquisition of data); furthermore, only eight values were employed in this case.

All $T_1$ values were determined from nonlinear least-squares analyses using a three-parameter fit program based on the FIRFT expression[19] and taking pulse imperfections (single-coil probe configurations) into account, i.e.

$$M_z(\tau) = M_0 - M_0[1 + \alpha\{1 - \exp(T_{Rep}/T_1)\}] \exp(-\tau/T_1)$$

Based on these fittings of experimental data, the errors in $T_1$ are within 2–5%; however, for the determinations of $T_1(^{15}N)$ at 2.3 T and $T_1(^{113}Cd)$ at 4.7 T, the errors are somewhat larger (5–10%). The evaluations of the anisotropic rotational diffusion constants for Py–Cd–TPP from the relaxation and solid-state chemical shift anisotropy data were performed by using computer programs based on the equations derived in the Theory section.

All chemical shifts are in ppm with the positive directions corresponding to lower shielding than the references. The following references were used: $Me_4Si$ (internal) for $^1H$ and $^{13}C$, $CH_3NO_2$ (external sample) for $^{15}N$, and 0.1 M $Cd(ClO_4)_2$ in $D_2O$ (external sample) for $^{113}Cd$ using a correction of 2.60 ppm for the difference in the lock frequencies for $CDCl_3$ and $D_2O$.

Solid-state $^{113}Cd-^1H$ cross-polarization (CP) NMR experiments, with an without magic angle spinning (MAS), were performed on a highly modified Bruker WP-200 spectrometer at frequencies of 44.40 and 200.13 MHz for $^{113}Cd$ and $^1H$, respectively. The modification of this spectrometer for solid-state NMR experiments is described in detail elsewhere.[23] The double-tuned probes and high-speed cylindrical sample spinners used for the MAS experiments are likewise described elsewhere.[24,25] A maximum rotor speed of about 4.0 kHz was employed and monitored by using a Tektronix Model 7L13 spectrum analyzer. A 90° $^{113}Cd$ pulse was 4 $\mu$s with either probe, corresponding to a rotating-frame $H_{1Cd}$ field of 66.2 G. The corresponding $H_{1H}$ field was adjusted to 14.7 in order to fulfill the Hartmann–Hahn condition.[26] The cross-polarization (CP) experiments were performed by using a single contact with flip-back of the $^1H$ magnetization.[27] For Cd–TPP and Py–Cd–TPP, the experimental conditions were respectively as follows: CP contact time, 2 and 1 ms; spectral width, 40 and 20 kHz; acquisition time, 0.1 s; recycle time of the experiments, 4 and 2 s. The line broadening for sensitivity enhancement was typically 88 Hz (2 ppm). The collected number of scans was 20 000–30 000 scans for the powder spectra and 800 scans for the MAS spectra. Solid-state $^{113}Cd$ chemical shifts in ppm are reported with respect to a sample of solid $Cd(ClO_4)_2 \cdot 6H_2O$. The chemical shift ($\delta$) scale is positive to lowering shielding while the shielding constant ($\sigma$) scale is positive to larger shielding. Calculations of the simulated MAS spectra were performed by using a program to be described elsewhere.[28]

The tuning of the high-resolution NMR probes for all spectrometers employed in this research was performed according to the procedure recently described.[29] For the solid-state measurements, probe tuning was accomplished under dynamic loading by the use of high-power dual directional couplers.

(20) H. J. Jakobsen and W. S. Brey, *J. Am. Chem. Soc.*, **101**, 774 (1979).
(21) O. W. Sørensen, S. Scheibye, S.-O. Lawesson, and H. J. Jakobsen, *Org. Magn. Reson.*, **16**, 322 (1981).
(22) S. L. Patt, private communication.
(23) R. R. Inners, F. D. Doty, A. R. Garber, and P. D. Ellis, *J. Magn. Reson.*, **45**, 503–9 (1981).
(24) F. D. Doty, R. R. Inners, and P. D. Ellis, *J. Magn. Reson.*, **43**, 399 (1981).
(25) F. D. Doty and P. D. Ellis, *Rev. Sci. Instrum.*, **52**, 12 (1981).
(26) (a) S. R. Hartmann and E. L. Hahn, *Phys. Rev.*, **128**, 2042 (1962); (b) A. Pines, M. Gibby, and J. S. Waugh, *J. Chem. Phys.*, **56**, 1776 (1972); **59**, 569 (1973).
(27) J. Tegenfeldt and V. Haeberlen, *J. Magn. Reson.*, **36**, 453 (1979).
(28) P. D. Ellis and H. Bildsøe, to be submitted for publication.
(29) P. Daugaard, H. J. Jakobsen, A. R. Garber, and P. D. Ellis, *J. Magn. Reson.*, **44**, 220 (1981).

## Theory

**Anisotropic Motion and Relaxation Parameters for Py–Cd–TPP.** Because of the special topology of cadmium *meso*-tetraphenylporphyrin (Cd–TPP), one would predict that the rotational diffusion of its pyridine complex (Py–Cd–TPP) in solution is anisotropic. Further, the diffusion tensor would have axial symmetry, such that $D_{xx} = D_{yy} = D_\perp$ and $D_{zz} = D_\parallel$. This statement is the result of two assumptions. First, Py–Cd–TPP is the principle species in solution. Second, there is fast, relatively unhindered rotation of the pyridine ligand about the Cd–N bond. The former assumption is reasonable, given the 10-fold excess of pyridine in the solution and the invariance of the $^{113}Cd$ chemical shift to added pyridine. The combination of these two assumptions puts the cadmium atom along a pseudo fourfold axis of symmetry. The theory of spin–lattice relaxation for molecules undergoing anisotropic diffusion has been an area of considerable interest.[30] Our discusson on the analysis of the anisotropic rotational diffusion for the porphyrin-ring skeleton of the Py–Cd–TPP complex will be separated into two parts. In the first part, we will discuss the motion of the nearly planar porphyrin ring. This will allow us to determine the perpendicular and parallel principle components of the diffusion tensor, $D_\perp$ and $D_\parallel$, respectively. In addition, the phenyl-ring substituents are executing rotational diffusion on a frame which is undergoing anisotropic diffusion. Importantly, these motions are uncorrelated. Thus, armed with the above-mentioned diffusion coefficients, we can determine the diffusion coefficient which characterized the motion of the phenyl rings.

Measurements of the anisotropic motion for planar systems by relaxation methods require two "spin-reporter" groups[31] which depend differently on $D_\perp$ and $D_\parallel$. In our case, the $^{13}C-^1H$ dipolar interaction for the protonated $\beta$ carbons of the "pyrrole" rings represents the in-plane vector and the $^{113}Cd$ shielding tensor provides the necessary perpendicular component. As stated above, the molecular symmetry of Py–Cd–TPP is such that its diffusion tensor can be described as axially symmetric. Further, since the cadmium is positioned on the pseudofourfold axis, the $^{113}Cd$ shielding tensor must effectively be axially symmetric. Therefore, any motion of the molecule about the pseudofourfold axis will *not* provide a chemical shift anisotropy (CSA) relaxation pathway for the $^{113}Cd$ spin-$^1/_2$ isotope.[32] Hence, a knowledge of the $^{113}Cd$ CSA ($\Delta\sigma$) and $T_1^{CSA}(^{113}Cd)$ will yield the perpendicular component of the diffusion tensor. The $^{13}C-^1H$ dipolar interaction of the $\beta$ carbon does not enjoy any special boundary conditions imposed by the symmetry of the molecule and, therefore, $T_1^{DD}(^{13}C)$ is a function of both diffusion constants, $D_\perp$ and $D_\parallel$. However, with the value of $D_\perp$, determined by the $^{113}Cd$ CSA relaxation processes, and $R_1^{DD}$ ($=1/T_1^{DD}$), the value of $D_\parallel$ can be determined.

(30) D. E. Woessner, *J. Chem. Phys.*, **36**, 1 (1962); D. E. Woessner, *ibid.*, **37**, 647 (1962); H. Shimizu, *ibid.*, **43**, 754 (1964); D. Wallach, *ibid.*, **47**, 5258 (1967); T. T. Bopp, *ibid.*, **47**, 3621 (1967); D. E. Woessner, B. S. Snowden, Jr., and E. T. Strom, *Mol. Phys.*, **14**, 265 (1968); W. T. Huntress, Jr., *J. Chem. Phys.*, **48**, 3524 (1968); W. T. Huntress, Jr., *J. Phys. Chem.*, **73**, 103 (1969); D. Wallach, and W. T. Huntress, Jr., *J. Chem. Phys.*, **50**, 1219 (1969); J. Jonas and T. M. Digennaro, *ibid.*, **50**, 2392 (1969); W. T. Huntress, *Adv. Magn. Reson.*, **4**, 1 (1970).
(31) R. L. Vold, R. R. Vold, and D. Canet, *J. Chem. Phys.*, **66**, 1202 (1977).
(32) If an axially symmetric shielding tensor ($\sigma_{xx} = \sigma_{yy} \neq \sigma_{zz}$) is subjected to a rotation about its unique axis, i.e.

$$\sigma' = R\sigma R^{-1}$$

where

$$R = \begin{pmatrix} \cos\theta & \sin\theta & 0 \\ -\sin\theta & \cos\theta & 0 \\ 0 & 0 & 1 \end{pmatrix}$$

then it is easily shown that the resulting shielding tensor is identical with the original tensor. Therefore, any motion about the unique axis of an axially symmetric tensor cannot provide a mechanism for chemical shift anisotropy relaxation for the nucleus in question.

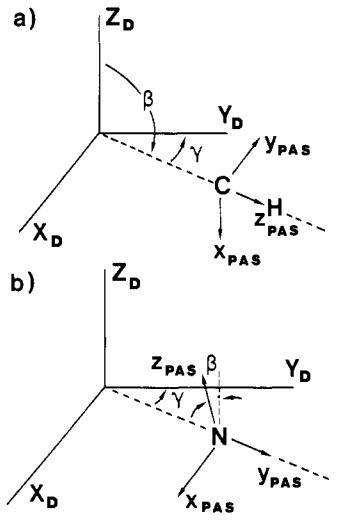


**Figure 2.** Definition of the various angles for the calculation of (a) the dipolar relaxation rate and (b) the chemical shift anisotropy relaxation rate. In both cases, we have taken advantage of the planarity of our system. This situation has allowed us to place the $Y_{pas}$ axis in the $X_D$, $Y_D$ diffusion plane. In part a the $Z_{pas}$ axis of the dipolar interaction lies along the dipole vector. A rotation about the $Y_{pas}$ axis through an angle $\beta$ brings the $Z_{pas}$ axis parallel to $Z_D$. A second rotation about the new $Z_{pas}$ axis through an angle $\gamma$ brings the two coordinate systems into congruency. In the case of the chemical shift tensor (b) the unique direction is less clearly defined. It is customary in planar molecules to choose the axis which is perpendicular to the plane of the molecule to be the unique axis. We have followed this convention. A rotation about the $Y_{pas}$ axis through an angle $\beta$ brings $Z_{pas}$ parallel to $Z_D$ (in our case $\beta = 0$). A rotation about the new $Z_{pas}$ axis through the angle $\gamma$ brings the two coordinate systems to congruency.

Spiess[33] has derived the necessary general relaxation equations required for analysis of the pertinent relaxation data. The results are

$$R_1^{CSA} = \gamma_I^2 B_0^2 g_2^{CS}(\omega) \qquad \text{with } \gamma_I B_0 = \omega \tag{1}$$

$$R_1^{DD} = \tfrac{4}{3}\gamma_I^2\gamma_S^2\hbar^2 S(S+1)[\tfrac{1}{3}g_2^D(\omega_I - \omega_S) + g_2^D(\omega_I) + 2g_2^D(\omega_I + \omega_S)] \tag{2}$$

where

$$g_2(\omega) = \sum_{k=-2}^{+2} \frac{c_{2k}\tau_{2k}}{1 + \omega^2\tau_{2k}^2} \tag{3}$$

In arriving at eq 1, we have ignored the contribution of $R_1^{CSA}$ by the antisymmetric components ($g_1^{CS}(\omega)$) of the shielding tensor. This approximation is valid for $^{13}C$[34] and is assumed to hold also for $^{113}Cd$. The symbols in eq 1 and 2 have their usual meanings. The "spectral density"[35] function, $g_2(\omega)$, can be evaluated via the tables of correlation times ($\tau_{1k}$), coefficients ($c_{1k}$), and coupling parameters ($\delta_\lambda$) given by Spiess[36] and by reference to Figure 2 for the definition of the various Euler angles. With these points in mind and with the simplication that $\eta_D = 0$ which is pertinent to the systems studied here, eq 1 and 2 can be rewritten as

$$R_1^{CSA} = \frac{1}{90}\gamma_I^2 B_0^2 \Delta\sigma^2 \left[ A\frac{\tau_2}{1+\omega^2\tau_2^2} + B\frac{\tau_1}{1+\omega^2\tau_1^2} + C\frac{\tau_0}{1+\omega^2\tau_0^2} \right] \tag{4}$$

where

$$A = 9\sin^4\beta - 6\eta\sin^2\beta\cos 2\alpha(\cos^2\beta + 1) + \eta^2[\cos^2 2\alpha(\cos^2\beta + 1)^2 + 4\sin^2 2\alpha\cos^2\beta] \tag{5}$$

$$B = 9\sin^2 2\beta + 6\eta\sin^2 2\beta\cos 2\alpha + \eta^2(\cos^2 2\alpha\sin^2 2\beta + 4\sin^2 2\alpha\sin^2\beta) \tag{6}$$

$$C = 3[(3\cos^2\beta - 1)^2 - 2\eta(3\cos^2\beta - 1)\sin^2\beta\cos 2\alpha + \eta^2\sin^4\beta\cos^2 2\alpha] \tag{7}$$

$$R_1^{DD} = \frac{3}{40r_6}\gamma_I^2\gamma_S^2\hbar^2[J(\omega_S - \omega_I) + 3J(\omega_I) + 6J(\omega_I + \omega_S)] \tag{8}$$

where

$$J(\omega) = \sin^4\beta\frac{\tau_2}{1+\omega^2\tau_2^2} + \sin^2 2\beta\frac{\tau_1}{1+\omega^2\tau_1^2} + \frac{1}{3}(3\cos^2\beta - 1)^2\frac{\tau_0}{1+\omega^2\tau_0^2} \tag{9}$$

Further

$$\tau_2 = [2D_\perp + 4D_\parallel]^{-1} \tag{10}$$

$$\tau_1 = [5D_\perp + D_\parallel]^{-1} \tag{11}$$

$$\tau_0 = [6D_\perp]^{-1} \tag{12}$$

For the case of $^{113}Cd$ CSA relaxation in Py–Cd–TPP the asymmetry parameter, $\eta$, is zero because the shielding tensor was found to be axially symmetric. Furthermore, the Euler angles $\alpha$ and $\beta$ are zero. Under these conditions $A = B = 0$ and $C = 12$; thus eq 4 reduces to

$$R^{CSA}(^{113}Cd) = \frac{2}{15}\omega_I^2\Delta\sigma^2\frac{\tau_0}{1+\omega_I^2\tau_0^2} \tag{13}$$

which is the usual expression cited for $R_1^{CSA}$.[37] We are also interested in the prediction of the $^{15}N$ shielding tensor for the nitrogens of the porphyrin ring. For the case of the $^{15}N$ CSA relaxation $\alpha = 0$ (or $\pi/4$) and $\beta = 0$; however, the $^{15}N$ shielding tensor cannot be assumed to be axially symmetric. With these conditions in mind, $A = 4\eta^2$, $B = 0$, and $C = 12$; thus, eq 4 reduces to:

$$R_1^{CSA}(^{15}N) = \frac{2}{45}\omega_I^2\Delta\sigma^2\left[\eta^2\frac{\tau_2}{1+\omega_I^2\tau_2^2} + \frac{3\tau_0}{1+\omega_I^2\tau_0^2}\right] \tag{14}$$

From a simple error analysis of eq 14, it is easily seen that it will usually be difficult to determine $\eta$ (a number between 0 and 1) from liquid-state relaxation data alone, e.g., from determinations of $R_1^{CSA}(^{15}N)$ at two magnetic field strengths and with a knowledge of $\tau_2$ and $\tau_0$. However, given $\tau_2$ and $\tau_0$ (i.e., $D_\parallel$ and $D_\perp$) and $T_1^{CSA}(^{15}N)$ at one frequency, one can usually predict a value for $\Delta\sigma$ within reasonable error limits from eq 14. On the other hand, $\eta$ will have to be determined from solid-state NMR experiments.

For the $^{13}C$–$^1H$ dipolar relaxation of the pyrrole C$\beta$ carbon, the angle $\beta$ is $\pi/2$ and therefore the expression for the spectral density function, $J(\omega)$ (eq 9) reduces to

$$J(\omega) = \frac{\tau_2}{1+\omega^2\tau_2^2} + \frac{1}{3}\frac{\tau_0}{1+\omega^2\tau_0^2} \tag{15}$$

Note that in this special case $J(\omega)$ is independent of $\tau_1$.

To properly describe $^{13}C$–$^1H$ dipolar relaxation for the carbons of the phenyl-ring substituents in Py–Cd–TPP, one must change the spectral density function $g_2(\omega)$ (eq 3) entering eq 2, because of the internal motion of this group. The following expression

(33) H. W. Spiess in "NMR Basic Principles and Progress", Vol. 15, P. Diehl, E. Fluck, R. Kosfeld, Eds., Springer-Verlag, New York, 1978; see the excellent discussion on pp 107–35 and Tables 4.9 and 4.10.

(34) This contribution, which cannot be determined experimentally, has been shown to be negligible for $^{13}C$; unpublished calculations by P. D. Ellis.

(35) Since $g_2(\omega)$ contains the coupling parameter $\delta_\lambda$, it does not represent a true spectral density. However, for an axially symmetric coupling tensor the spectral densities and coupling parameters can easily be separated.

(36) Reference 33, Table 4.9, p 133.

(37) T. C. Farrar and E. D. Becker, "Pulse and Fourier Transform NMR", Academic Press, New York, 1971, p 59.

can be derived following the treatment by Wallach[30d] with reference to Figure 3

$$g_2(\omega) = \sum_{j=-2}^{+2} \sum_{k=-2}^{+2} D_{oj}^{(2)} D_{oj}^{(2)*} c_{2k} \frac{\tau_{jk}}{1 + \omega^2 \tau_{jk}^2} \quad (16)$$

with

$$\frac{1}{\tau_{jk}} = \frac{j^2}{\tau^*} + \frac{1}{\tau_{2k}} \quad (17)$$

leading to

$$g_2(\omega) = \frac{1}{4}(3\cos^2\theta - 1)^2 \sum_{k=-2}^{+2} c_{2k} \frac{\tau_{2k}}{1 + \omega^2 \tau_{2k}^2} + \frac{3}{4}\sin^2 2\theta \sum_{k=-2}^{+2} c_{2k} \frac{\left(\frac{1}{\tau^*} + \frac{1}{\tau_{2k}}\right)^{-1}}{1 + \omega^2\left(\frac{1}{\tau^*} + \frac{1}{\tau_{2k}}\right)^{-2}} + \frac{3}{4}\sin^4\theta \sum_{k=-2}^{+2} c_{2k} \frac{\left(\frac{4}{\tau^*} + \frac{1}{\tau_{2k}}\right)^{-1}}{1 + \omega^2\left(\frac{4}{\tau^*} + \frac{1}{\tau_{2k}}\right)^{-2}} \quad (18)$$

where $\theta$ is defined in Figure 3 and $(\tau^*)^{-1} = D^*$ is the diffusion constant describing the rotational motion of the phenyl-ring substituents around the C1–C4 axis relative to the porphyrin-ring skeleton. From eq 18 it can be seen, when $\theta$ is equal to zero, that is, when the C–H vector lies along the internal rotational diffusion axis, the expression for $g_2(\omega)$ reduces to eq 3. Therefore, the D–D relaxation for this C–H vector is independent of the internal motion. Further, for $\theta = \pi/3$ the expression for $g_2(\omega)$ (eq 18) is identical with the case when $\theta = 2\pi/3$. This condition is important for the symmetry of the phenyl ring and is clear from the trigonometry in eq 18. With eq 18 at hand, we can derive a new expression for the spectral density function $J(\omega)$, i.e.

$$J(\omega) = \frac{1}{4}(3\cos^2\theta - 1)^2\left[\sin^4\beta \frac{\tau_2}{1 + \omega^2\tau_2^2} + \sin^2 2\beta \frac{\tau_1}{1 + \omega^2\tau_1^2} + \frac{1}{3}(3\cos^2\beta - 1)^2 \frac{\tau_0}{1 + \omega^2\tau_0^2}\right] + \frac{3}{4}\sin^2 2\theta\left[\sin^4\beta \frac{\tau_2'}{1 + \omega^2\tau_2'^2} + \sin^2 2\beta \frac{\tau_1'}{1 + \omega^2\tau_1'^2} + \frac{1}{3}(3\cos^2\beta - 1)^2 \frac{\tau_0'}{1 + \omega^2\tau_0'^2}\right] + \frac{3}{4}\sin^4\theta\left[\sin^4\beta \frac{\tau_2''}{1 + \omega^2\tau_2''^2} + \sin^2 2\beta \frac{\tau''}{1 + \omega^2\tau_1''^2} + \frac{1}{3}(3\cos^2\beta - 1)\frac{\tau_0''}{1 + \omega^2\tau_0''^2}\right] \quad (19)$$

where $\tau_2$, $\tau_1$, and $\tau_0$ are defined as before in eq 10–12 and

$$\tau_2' = [D^* + 2D_\perp + 4D_\parallel]^{-1} \quad (20)$$

$$\tau_1' = [D^* + 5D_\perp + D_\parallel]^{-1} \quad (21)$$

$$\tau_0' = [D^* + 6D_\perp]^{-1} \quad (22)$$

$$\tau_2'' = [4D^* + 2D_\perp + 4D_\parallel]^{-1} \quad (23)$$

$$\tau_1'' = [4D^* + 5D_\perp + D_\parallel]^{-1} \quad (24)$$

$$\tau_0'' = [4D^* + 6D_\perp]^{-1} \quad (25)$$

In eq 19 the angle $\beta$, as before, is equal to $\pi/2$. The diffusion constant $D^*$ describes the motion (within the diffusion model) of the phenyl rings. Equations 23–25 change if one employs a symmetry jump model for the phenyl-ring motion. With reference to the discussions by Wallach,[30d] one can convince oneself that $4D^*$ should be replaced by simply $D^*$ for the jump model. Here $D^*$ denotes the lifetime for a particlar orientation of phenyl rings. Other models can be envisioned; however, we will limit our discussion to the diffusion model given by eq 23–25.

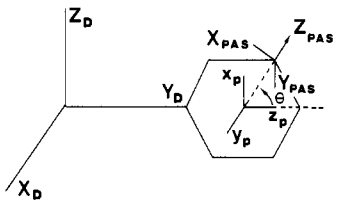


**Figure 3.** Definition of the various angles for the calculation of the dipolar relaxation rate for the phenyl ring undergoing internal motion about $Z_p$, the $Z$ axis of the phenyl ring. The CH vector makes an angle $\theta$ with the $Z_p$ axis. In our case, we can bring the phenyl coordinate system to congruency with the diffusion frame with Euler angles $\alpha = 0$, $\beta = \pi/2$, $\gamma = \pi/2$. In the more general case where the phenyl ring is tilted ($\beta \neq \pi/2$) and off axis ($\gamma \neq \pi/2$) then eq 17 is still valid, as long as the diffusion tensor is still axially symmetric. Under the condition of axial symmetry, the expressions for $R_1^{CSA}$ and $R_1^{DD}$ are independent of the angle $\alpha$.

The effect of the anisotropic motion on the $^{13}C$-$\{^1H\}$ nuclear Overhauser effect (NOE), for the pyrrole C$\beta$ carbon as well as the phenyl-ring carbons, may be derived from the general equation

$$\eta = T_1\hbar^2\gamma_S^3\gamma_I[2g_2^D(\omega_I + \omega_S) - 1/3g_2^D(\omega_I - \omega_S)] \quad (26)$$

given by Spiess[38] and pertinent to the NOE for $I = {}^1/_2$, $S = {}^1/_2$ two-spin system ($I$-$\{S\}$). Using eq 2, one may derive the following expression for the maximum NOE (100% D–D relaxation)

$$\eta_{max} = \frac{\gamma_S}{\gamma_I} \frac{2J(\omega_I + \omega_S) - {}^1/_3J(\omega_S - \omega_I)}{{}^1/_3J(\omega_S - \omega_I) + J(\omega_I) + 2J(\omega_S + \omega_I)} \quad (27)$$

where the spectral density functions $J(\omega)$ of eq 9 and 19, with $\beta = \pi/2$, apply for the C$\beta$ carbon and phenyl-ring carbons, respectively.

## Results and Discussions

**Chemical Shifts and Spin–Spin Coupling Constants.** The chemical shifts, signs, and magnitudes of the spin–spin coupling constants determined for the four different spin-1/2 nuclei ($^{113}Cd$, $^{15}N$, $^{13}C$, and $^1H$) of the pyridine complex of $^{113}Cd$–[$^{15}N_4$]TPP are summarized in Table I. A brief discussion on these parameters, as obtained from the individual multinuclear NMR spectra, is given in the following paragraphs.

**$^{113}Cd$ NMR Spectra.** The proton-decoupled $^{113}Cd$ NMR spectrum of **1** (0.02 M solution in $CDCl_3$) at 9.4 T (88.78 MHz) is shown in Figure 4a and appears as a 1:4:6:4:1 quintet with $|^1J(^{113}Cd–^{15}N)| = 150.1$ Hz at $\delta = 426.8$ ppm and a $^{113}Cd$ line width of 1.0 Hz. In the proton-coupled $^{113}Cd$ spectrum (Figure 4b) the quintet lines show up as fairly well-resolved first-order multiplets which can be ascribed to four-bond $^{113}Cd$–$^1H$ spin–spin coupling to the eight H$\beta$ protons, $|^4J(^{113}Cd–H\beta)| = 5.0$ Hz; the corresponding H$\beta$–$^{113}Cd$ doublet in the $^1H$ spectrum is observed at 8.05 ppm. In addition, the $^{113}Cd$ spectrum of the minor abundant isotopomer Py–$^{113}Cd$–[$^{15}N_3$,$^{14}N$]TPP (17%) is observed as a 1:3:3:1 quartet in the spectra of Figure 4. However, the line width of the resonances for this isotopomer are larger (approximately 8–12 Hz) than for **1** because of the presence of the $^{14}N$ spin-1 quadrupole nucleus. The observed $^{113}Cd$ chemical shift of 426.8 ppm is in the region expected[7–9] for covalent cadmium complexes with coordination to nitrogen ligands. The magnitude of the observed $^{113}Cd$–$^{15}N$ coupling constant, $|^1J(^{113}Cd–^{15}N)| = 150.1$ Hz, may be compared to the value of $|^1J(^{111}Cd–^{15}N)| = 142.5$ Hz, determined indirectly from $^1H$ spectra using $^1H$-$\{^{111}Cd\}$

(38) Reference 33, p 179.

Table I. $^{113}Cd$, $^{15}N$, $^{13}C$, $^{1}H$ Chemical Shifts[a] and Magnitudes and Signs of Spin–Spin Coupling Constants[b] Determined for the Pyridine Adduct of $^{113}Cd$–[$^{15}N_4$]TPP from $^{113}Cd$, $^{15}N$, $^{13}C$, and $^{1}H$ NMR Spectra

| | obsd nuclei (x) | | | |
|---|---|---|---|---|
| | $^{113}Cd$ | $^{15}N$ | $^{13}C$[c] | $^{1}H$ |
| $\delta$(x) | 426.8 | −170.9 | 150.6 (Cα) | |
| | | | 131.4 (Cβ) | 8.77 |
| | | | 121.3 (Cγ) | |
| $^{1}J(^{113}Cd–^{15}N)$[d] | +150.1 | +150.1 | | |
| $\lvert^{2}J(^{113}Cd–C\alpha)\rvert$[e] | | | 2.6 | |
| $^{3}J(^{113}Cd–C\beta)$ | | | −12.2 | |
| $^{3}J(^{113}Cd–C\gamma)$ | | | −10.7 | |
| $^{4}J(^{113}Cd–H\beta)$ | −5.0 | | | −5.0 |
| $\lvert J(^{15}N–C\alpha)\rvert$[f] | | | <2.0 | |
| $\lvert^{3}J(^{15}N–C\beta)\rvert$ | | | <0.5 | |
| $\lvert J(^{15}N–C\gamma)\rvert$[g] | | | <4.0 | |
| $\lvert^{3}J(^{15}N–H\beta)\rvert$[h] | | ~0.5 | | |
| $^{2}J(C\beta–H\beta')$ | | | 5.1 | |

[a] Chemical shifts are in ppm (±0.1 ppm; $^{1}H$ NMR: ±0.01 ppm) with the positive direction to lower shielding from the references which are as follows: $^{113}Cd$, external 0.1 M $Cd(ClO_4)_2$ in $D_2O$; $^{15}N$, external $CH_3NO_2$; $^{13}C$, internal $Me_4Si$; $^{1}H$, internal $Me_4Si$. [b] Coupling constants are in hertz (±0.1 Hz). [c] Only the porphyrin-ring $^{13}C$ chemical shifts are shown; the $^{13}C$ chemical shifts for the phenyl-group and pyridine carbons are as follows: C1, 143.8; C2, 134.7; C3, 126.0; C4, 126.8; C2(py), 149.3; C3(py), 123.5; and C4(py), 135.8 ppm. [d] The value $^{1}J(^{113}Cd–^{15}N)$ = 150.1 Hz is observed at 30 °C; at the slightly higher temperature. 33 °C, obtained with continuous $^{1}H$ decoupling this value increases to 150.3 Hz. [e] Observed as a doublet for the pyridine adduct of $^{113}Cd$–[$^{14}N_4$]TPP (2). [f] $\lvert^{1}J(^{15}N–C\alpha)\rvert$ and $\lvert^{3}J(^{15}N–C\alpha)\rvert$ are both less than 2 Hz. [g] The sum $\lvert^{2}J(^{15}N–C\gamma) + {}^{4}J(^{15}N–C\gamma)\rvert$ is less than 4.0 Hz as judged from spectral simulations of the spectrum in Figure 6. [h] Estimated from the coupled $^{15}N$ spectrum and $^{15}N$–{$^{1}H$} SPT experiments (e.g., Figure 5).

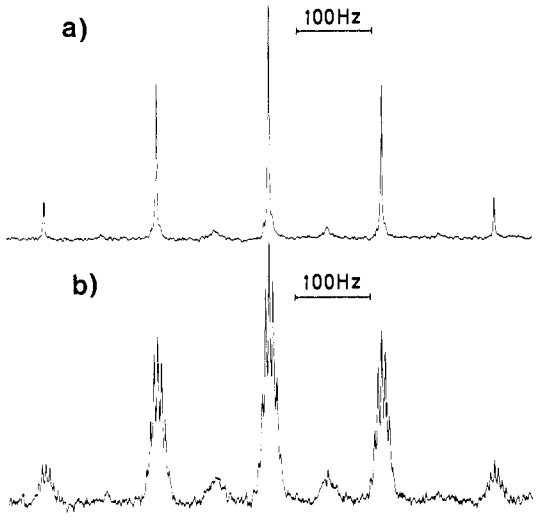


**Figure 4.** $^{113}Cd$ NMR spectra (88.78 MHz) or a 0.02 M solution of the pyridine adduct of $^{113}Cd$–[$^{15}N_4$]TPP, Py–Cd–TPP, in $CDCl_3$: (a) proton decoupled, 250 transients; (b) proton coupled, 600 transients. A flip angle of 45° has been used for both spectra.

and $^{1}H$–{$^{15}N$} INDOR techniques, for the $^{111}Cd/^{15}N$ multiply labeled complex **1**.[39] The calculated coupling $^{1}J(^{113}Cd–^{15}N)$(calcd) = $(\gamma_{^{113}Cd}/\gamma_{^{111}Cd})^{1}J(^{111}Cd–^{15}N)$(obsd) = 148.1 Hz is in good agreement with our experimental value which, however, is of higher accuracy because of the much narrower line obtained for the proton-decoupled $^{113}Cd$ spectrum. The determination of a positive spin for $^{1}J(^{113}Cd–^{15}N)$ was carried out from $^{15}N$ and $^{13}C$ experiments (vide infra). Despite the fact that the Cd–N bond is commonly encountered, especially in biological studies using cadmium as a probe, we are aware of only three other reports of one-bond Cd–N coupling constants. For the Cd(II)–EDTA complex, it has been reported that $\lvert^{1}J(^{113}Cd–^{15}N)\rvert$ = 81 Hz,[40] whereas, for the two cadmium–glycine complexes, $Cd^{II}Gly^{+}$ and $Cd^{II}Gly_2$, $\lvert^{1}J(^{113}Cd–^{1N})\rvert$ = 170 and 165 Hz, respectively, have been observed upon supercooling to −40 °C.[9b] In cadmium-substituted carbonic anhydrase, Sudmeier and co-workers[12k] have observed couplings as large as 190 and 210 Hz.

It should be noted that proton decoupling may be applied continuously for the observation of the $^{113}Cd$ spectrum in Figure 4a because of the very small $^{113}Cd$–{$^{1}H$} NOE at 88.78 MHz (vide infra) and therefore negligibly small reduction of $^{113}Cd$ intensities ($\gamma_{^{113}Cd} < 0$). Furthermore, the proton-decoupled $^{113}Cd$ NMR spectrum of **1** (Figure 4a) may actually be observed in less than 1 min, using only a few transients owing to the reasonably short relaxation time $T_1(^{113}Cd)$ = 10.3 s and the narrow $^{113}Cd$ line width. These observations are in contrast to our early preliminary 22.19-MHZ $^{113}Cd$ investigations on Lewis base adducts of Cd–TPP possessing 96% $^{113}Cd$ enrichment and $^{14}N/^{15}N$ isotopically normal "pyrrole" (**2**). Much longer accumulation times (5–20 h) were required in these studies because of excessively long $T_1(^{113}Cd)$ relaxation times combined with the broad (ca. 50–80 Hz) $^{113}Cd$ resonances. Actually, in an earlier communication[13b] on the detection of the $^{113}Cd$ resonance for Lewis base adducts of **2**, the reported $^{113}Cd$ line widths (ca. 80 Hz) were too broad to allow the effect of proton decoupling to be detected. However, it is noteworthy that the $^{113}Cd$ resonance for the pyridine complex of **2** observed in this study at 88.78 MHz using proton decoupling appears as a singlet having a line width of 23 Hz and may be observed using only one to four transients. The effect of $^{14}N$ decoupling, using $^{113}Cd$–{$^{1}H$,$^{14}N$} triple-resonance techniques, on the width of this resonance remains yet to be explored.

Although the isotropic $^{113}Cd$ chemical shift for "free, unliganded" Cd–TPP (**1**) has been obtained from our solid-state NMR studies (vide infra), several attempts have been made to observe the $^{113}Cd$ resonances in the liquid state using a saturated solution of Cd–TPP in $CDCl_3$. However, despite 20 h of accumulation, we have so far not observed the $^{113}Cd$ resonances for "unliganded" Cd–TPP, which is almost insoluble in chloroform (estimated to be less than 0.5 mM) and furthermore shows pronounced aggregation in solution. The highly structured aggregates formed at the concentrations of most NMR measurements have been shown to cause markedly irreproducible results in $^{13}C$ NMR.[14b]

**$^{15}N$ NMR Spectra.** Detailed $^{15}N$ NMR investigations including relaxation studies were performed for the pyrrole nitrogens of Py–Cd–TPP (**1**) at both 40.55 MHz (9.4 T) and 10.14 MHz (2.3 T). Because of the negligibly small $^{15}N$–{$^{1}H$} NOE ($\gamma_{^{15}N} < 0$) and much more favorable $^{15}N$ relaxation rate at 40.55 MHz (vide infra, Table III), the proton-decoupled $^{15}N$ spectrum is obtained most conveniently at this frequency employing continuous broad-band decoupling. Determination of the proton-decoupled $^{15}N$ spectrum at 10.14 MHz, using conventional FT methods, requires small flip angles and gated decoupling techniques owing to the unfavorable $T_1(^{15}N)$ and NOE ($\eta$ = −0.8 to −0.9). However, *J*-polarization transfer via the selective population transfer (SPT) method[20] can be applied most profitably for the observation of the $^{15}N$ spectrum at low frequency. The proton-decoupled $^{15}N$ spectrum of a 23 mM solution of **1** may be observed after only a few (one to four) transients at 40.55 MHz and appears as a sharp doublet ($\lvert^{1}J(^{113}Cd–^{15}N)\rvert$ = 150.1 Hz) at $\delta$ = −170.9 ppm. The $^{15}N$ line width of the decoupled spectrum is 0.2 Hz at either magneitc field. For the proton-coupled $^{15}N$ spectrum, the width of the doublet lines simply increases to 1.2 Hz caused mainly by three-bond $^{15}N$–$^{1}H$ coupling to the Hβ protons ($\lvert^{3}J(^{15}N–H\beta)\rvert$ = 0.5 Hz). However, no multiplet fine structure is apparent in the $^{15}N$ resonance lines and no attempts were made to resolve the small $^{3}J(^{15}N–H\beta)$ doublet splitting in the $^{1}H$ spectrum for Hβ (a doublet, $^{4}J(^{113}Cd–H\beta)$ = 5.0 Hz). Despite the small magnitude

(39) D. D. Dominguez, M. M. King, and H. J. C. Yeh, *J. Magn. Reson.*, **32**, 161 (1978).

(40) R. Hagen, J. P. Warren, D. H. Hunter, and J. D. Roberts, *J. Am. Chem. Soc.*, **95**, 5712 (1973).

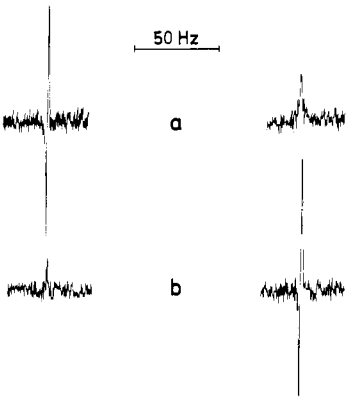


**Figure 5.** $^{15}N$–{H$\beta$} SPT FT NMR spectra (10.14 MHz) of the $^{15}N$–$^{113}Cd$ doublet ($^1J(^{113}Cd–^{15}N)$ = 150.1 Hz) for a 0.02 M solution of Py–Cd–TPP (**1**) in $CDCl_3$. (a) SPT $\pi$ pulse applied at the high-frequency line for H$\beta$–$^{113}Cd$ doublet ($|^4J(^{113}Cd–H\beta)|$ = 5.0 Hz) in the H$\beta$ spectrum. (b) SPT $\pi$ pulse applied 5.0 Hz to lower frequency than for part a. a and b represent accumulations of 100 transients each obtained by using a $^{15}N$ flip angle of 90°.

for $^3J(^{15}N–H\beta)$, we found it possible to experimentally employ this coupling constant for *J*-polarization transfer in the $^{15}N$ spectrum using SPT. This enabled the determination of the relative sign for the two reduced coupling constants $^1K(^{113}Cd–^{15}N)$ and $^4K(^{113}Cd–H\beta)$, where $K(ij) = 4\pi^2J(ij)/(h\gamma_i\gamma_j)$. Reference to the $^{15}N$–{H$\beta$} SPT experiments in Figure 5 shows that $^1K(^{113}Cd–^{15}N)$ $^4K(^{113}Cd–H\beta) > 0$ and $|^3J(^{15}N–H\beta)| \approx 0.5$ Hz. The sign of $^4K(^{113}Cd–H\beta)$ required for obtaining the absolute sign of $^1K(^{113}Cd–^{15}N)$ was determined from $^{13}C$ NMR experiments (vide infra). Furthermore, the experiments in Figure 5 show that, employing the SPT method, one may even achieve *J*-polarization transfer using very small coupling constants. Proton polarization transfer employing similarly small *J* couplings has so far not been performed by using the alternative method of the INEPT[41] pulse sequence and may prove difficult to perform with this technique.

The $^{15}N$ chemical shifts observed for Py–Cd–TPP is very similar to that determined by Gust and Roberts[15d,15h] for the zinc complex of $[^{15}N_4]$TPP, Zn–$[^{15}N_4]$TPP[42] (–185.2 ppm relative to external 0.1 M $D^{15}NO_3$; i.e., ca. –178 ppm relative to external $CH_3NO_2$[43]). Further, the $^{15}N$ shift does not differ significantly from that reported for bis(pyridine) complex of $^{57}Fe$–$[^{15}N_4]$TPP[15f] (–169.7 ppm relative to external $H^{15}NO_3$) and that for the pyridine adduct of cadmium octaethylporphyrin-$^{15}N_4$[15g] (–173.1 ppm relative to external $NH_4{}^{15}NO_3$). It is interesting to note that the $^{15}N$ chemical shifts for the metalloporphyrins quoted here in the region of those for the nitrogens of "chlorophyll *a*" as measured indirectly by Katz et al.[15a] Finally, it is noteworthy that the $^{15}N$ sensitivity observed at 9.4 T for the $^{15}N$ NMR experiments in this investigation, as compared to earlier $^{15}N$ studies on metalloporphyrins,[15] appears much more promising for future applications of this nuclide as a probe in NMR studies of porphyrin/metalloporphyrin derivatives.

**$^{13}C$ NMR Spectra.** The assignment of the proton-decoupled $^{13}C$ NMR spectrum for Py–Cd–TPP (**1**) followed from conventional methods such as the proton-coupled $^{13}C$ spectrum and selective proton decoupling experiments, but also from the magnitudes of the $^{13}C$–$^{113}Cd$ and $^{13}C$–$^{15}N$ coupling constants. The $^{13}C$ chemical shifts and their assignment (Table I) agree perfectly with those reported by Abraham et al.[14a] for isotopically normal Cd–TPP using pyrrolidine as a fifth ligand. Distinction between the $^{13}C$–$^{113}Cd$ and $^{13}C$–$^{15}N$ coupling constants in the proton-decoupled $^{13}C$ spectrum followed immediately from a comparison with the spectrum of the Py–Cd–TPP isotopomer possessing 96% $^{113}Cd$ enrichment and $^{14}N/^{15}N$ isotopically normal pyrrole nitrogens. In principle, the proton-decoupled $^{13}C$ spectra for the two quaternary C$\alpha$ and C$\gamma$ (meso carbon) carbons in **1** constitute the X parts of AA'BB'MX (A = B = $^{15}N$, M = $^{113}Cd$) spin systems. Because of the second-order nature of these spin systems and the unknown magnitudes and signs for the two different types of $^{15}N$–$^{15}N$ coupling constants, no efforts were attempted to analyze the complex spectra for these carbons (e.g., Figure 6). Thus, only upper limits for the magnitudes of the $^{13}C$–$^{15}N$ coupling constants determined from the widths of appropriate multiplets for C$\alpha$ and C$\beta$ are reported.

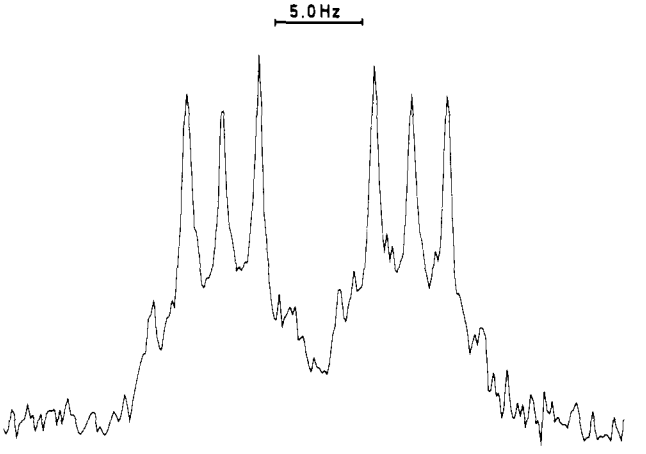


**Figure 6.** Proton-decoupled $^{13}C$ NMR spectrum for the C$\gamma$ carbon in Py–Cd–TPP (**1**).

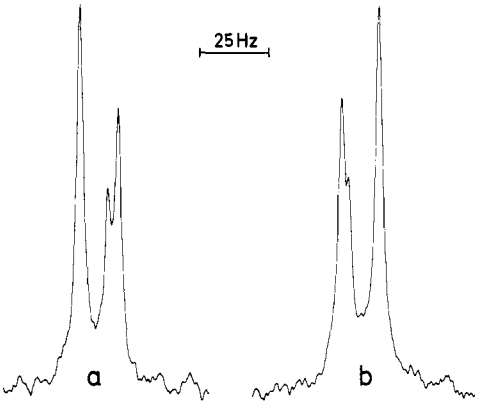


**Figure 7.** Single-frequency proton-decoupled $^{13}C$ NMR spectra for the C$\beta$ carbon in Py–Cd–TPP (**1**). (a) Irradiation at 2.5 Hz to higher frequency than the H$\beta$ chemical shift and (b) irradiation at 2.5 Hz to lower frequency than the H$\beta$ chemical shift ($|^4J(^{113}Cd–H\beta)|$ = 5.0 Hz). The experiments show that $^3K(^{113}Cd–H\beta) > 0$.

The determination of the absolute sign for the one-bond $^{113}Cd$–$^{15}N$ coupling constant, observed in the $^{113}Cd$ and/or $^{15}N$ spectra, was finally achieved by establishing the sign of the product $^3K(^{113}Cd–^{13}C\beta)$ $^4K(^{113}Cd–H\beta)$ from the C$\beta$ spectrum. Because of the relatively large magnitude for $|^4J(^{113}Cd–H\beta)|$ = 5.0 Hz), the sign for this product is most readily obtained by using the $^{13}C$–{$^1H$} off-resonance/selective decoupling techniques described elsewhere.[44] Thus, with reference to the C$\beta$ spectra in Figure 7 obtained by using selective decoupling of the one-bond $^{13}C$–$^1H$ coupling constant for definite $^{113}Cd$ spin states, it is observed that $3K(^{113}Cd–^{13}C\beta)$ $^4K(^{113}Cd–H\beta) > 0$. The relative magnitudes of the two- and three-bond $^{113}Cd$–$^{13}C$ couplings for **1** are in accord with $|^3J(^{113}Cd–^{13}C) > 0$ has been established. Therefore, assuming

(41) R. Freeman and G. Morris, *J. Am. Chem. Soc.*, **101**, 760 (1979).
(42) From the work reported in reference 15d it is unclear whether Zn–$[^{15}N_4]$TPP (5.6 mM in chloroform) was investigated as the unliganded complex or in the form of an adduct with a Lewis base.
(43) (a) G. C. Levy and R. L. Lichter, "Nitrogen-15 Nuclear Magnetic Resonance Spectroscopy", Wiley, New York, 1979; (b) G. T. Martin, M. L. Martin, and J.-P. Gouesnard in "NMR Basic Principles and Progress", Vol. 18, P. Diehl, E. Fluck, and R. Kosfeld, Eds., Springer-Verlag, New York, 1981.
(44) H. J. Jakobsen, T. A. Bundgaard, and R. S. Hansen, *Mol. Phys.*, **23**, 197 (1972).
(45) C. J. Turner and R. F. M. White, *J. Magn. Reson.*, **26**, 1 (1977).

$3K(^{113}Cd-C\beta) > 0$ for **1**, we concluded that $^{4}K(^{113}Cd-^{H}\beta) > 0$ and thus, with the results from the $^{15}N$ NMR experiments (Figure 5), that $^{1}K(^{113}Cd-^{15}N) > 0$. From these results, we predict the sign of one-bond $^{113}Cd-^{15}N$ coupling constants reported elsewhere[9b,40] to be positive as well. Finally, it is noted that the magnitudes of the two- and three-bond $^{113}Cd-^{13}C$ couplings across a nitrogen atom ($^{2}J(^{113}Cd-^{13}C\alpha)$, $^{3}J(^{113}Cd-^{13}C\beta)$, and $^{3}J(^{113}Cd-^{13}C\gamma)$) determined for **1** are similar to those obtained for these types of couplings in Cd(II)-EDTA.[8]

For some time there has been an increasing realization that the pyrrole molecule is an appropriate model for pyrrolic rings in metalloporphyrins. This is probably best illustrated from a comparison of the bond lengths. For the pyrrole rings in porphyrins, the bond lengths[46] are approximately N-C$\alpha$ 1.37 Å, C$\alpha$-C$\beta$ 1.44 Å, and C$\beta$-C$\beta'$ 1.36 Å while the corresponding pyrrole values are 1.38, 1.37, and 1.43 Å.[47] This difference in the nature of the pyrrole rings is also reflected in the magntidues of the $^{13}C-^{15}N$ coupling constants (Table I). For pyrrole-$^{15}N$ it has been reported[48] that $^{1}J(^{13}C\alpha-^{15}N) = -12.97$ Hz and $^{2}J(^{13}C\beta-^{15}N) = -.392$ Hz. The magnitudes of the $^{13}C-^{15}N$ couplings for **1** are much smaller and are more similar to those obtained for heteroaromatics with "pyridine-like" nitrogen atoms (trigonal $sp^2$ hybridized nitrogen).[49] Especially this holds for $^{1}J(^{13}C\alpha-^{15}N)$ which is comparable to the value observed for pyridine-$^{15}N$;[50] $^{1}J(^{13}C\alpha-^{15}N) = +0.62$ Hz, $^{2}J(^{13}C\beta-^{15}N) = +2.53$ Hz, and $^{3}J(^{13}C\gamma-^{15}N) = -3.85$ Hz. Finally, the shorter bond length, and therefore more double-bond character for the C$\beta$-C$\beta'$ bond in **1** as compared to pyrrole, is reflected in the magnitude for the two-bond $^{13}C\beta-H\beta'$ couplings. For **1** $^{2}J(C\beta-H\beta') = +5.1$ Hz while for pyrrole[48] $^{5}J(C\beta-H\beta') = +4.61$ Hz.

**Solid-State $^{113}$Cd NMR Spectra.** Cross-polarization (CP) solid-state $^{113}$Cd NMR spectra of "free" Cd-TPP and its pyridine-$^{15}N$ adduct, Py-Cd-TPP, have been investigated with and without magic angle spinning (MAS) and have afforded the principle components of the $^{113}$Cd shielding tensors and the isotropic $^{113}$Cd shifts for the two species. The derivation of these data were performed with the main purposes of (i) a determination of the effects that pyridine ligand coordination has upon the $^{113}$Cd chemical shift and a qualitative evaluation of the structural factors that give rise to this chemical shift; (ii) a determination of the anisotropy in the motion ($\rho = D_{\parallel}/D_{\perp}$) for Py-Cd-TPP in solution as it relates to the spin-lattice relaxation parameters and for which $^{113}$Cd CSA relaxation provides the necessary perpendicular component, $D_{\perp}$ (vide supra). With respect to i it should be borne in mind that the isotropic $^{113}$Cd chemical shift difference for Cd-TPP and Py-Cd-TPP cannot be obtained from liquid-state NMR because of the low solubility/aggregation for pure Cd-TPP.

The *powder pattern* obtained from a CP $^{113}$Cd NMR spectrum of a powdered sample without MAS yield information about the principle components of the chemical shift tensor ($\sigma_{xx}$, $\sigma_{yy}$, and $\sigma_{zz}$).[51-53] For a nonaxially symmetric shielding tensor, with $\sigma_{xx} < \sigma_{yy} < \sigma_{zz}$, the shielding anisotropy, $\Delta\sigma$, is defined as

$$\Delta\sigma = \sigma_{zz} - 1/2(\sigma_{xx} + \sigma_{yy}) \tag{28}$$

Under the conditions of magic angle spinning of a solid powder sample, one can directly measure the isotropic average value, $\bar{\sigma}$, where

$$\bar{\sigma} = \tfrac{1}{3}(\sigma_{xx} + \sigma_{yy} + \sigma_{zz}) \tag{29}$$

The value equals the isotropic chemical shift ($\delta$) observed in the liquid state under the influence of random tumbling motions. Finally, the asymmetry parameter $\eta$ ($0 \le \eta \le 1$) entering eq 14 is defined as[51-53]

$$\eta = \frac{\sigma_{yy} - \sigma_{xx}}{\delta} = \frac{\sigma_{yy} - \sigma_{xx}}{\frac{2}{3}\Delta\sigma} \tag{30}$$

where $\delta = \frac{2}{3}\Delta\sigma$ is the CSA coupling parameter. Combining eq 28-30 yields the following useful relationships for the principle components of the shielding tensor

$$\sigma_{xx} = \bar{\sigma} - \tfrac{1}{3}\Delta\sigma(1 + \eta) \tag{31}$$

$$\sigma_{yy} = \bar{\sigma} - \tfrac{1}{3}\Delta\sigma(1 - \eta) \tag{32}$$

$$\sigma_{zz} = \bar{\sigma} + \tfrac{2}{3}\Delta\sigma \tag{33}$$

For the axially symmetric shielding tensor, i.e., $\sigma_{xx} = \sigma_{yy} = \sigma_{\perp}$ and $\sigma_{zz} = \sigma_{\parallel}$, the asymmetry parameter (eq 30) $\eta = 0$ and the shielding anisotropy (eq 28) is given by

$$\Delta\sigma = \sigma_{\parallel} - \sigma_{\perp} \tag{34}$$

Similarly for the axially symmetric case, the isotropic value (eq 29) reduces to

$$\bar{\sigma} = \tfrac{1}{3}(\sigma_{\parallel} + 2\sigma_{\perp}) \tag{35}$$

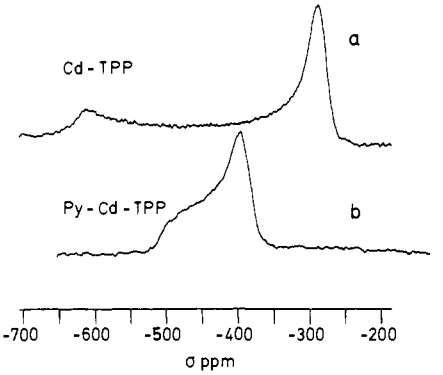


**Figure 8.** Cross-polarization (CP) solid-state $^{113}$Cd NMR powder spectra of (a) "free" Cd-TPP and (b) the pyridine-$^{15}N$ adduct of Cd-TPP. The shielding constant ($\sigma$) scale is positive to larger shieldings and is referred to a sample of solid $Cd(ClO_4)_2 \cdot 6H_2$).

CP $^{113}$Cd powder spectra of Cd-TPP[54a] and Py-Cd-TPP[54b] are shown in Figure 8. The MAS spectra were obtained from high-speed sample spinning at a maximum rate of 4.0 kHz about an axis oriented at 54.7° with respect to the static magnetic field. Spinning sidebands, with a separation of ±4.0 kHz, are clearly observable in the CP MAS spectrum of Cd-TPP (Figure 9) but are absent in the MAS spectrum for Py-Cd-TPP (not shown). The complexity of spinning sidebands can be avoided only if the spinning rate is comparable to or larger than the chemical shift anisotropy (expressed in frequency units). Obviously, this is not possible for Cd-TPP with a spinning rate of 4.0 kHz at a field of 4.7 T. Generally, the line width obtained in a MAS experiment is determined by instrumental limitations such as a magnet inhomogeneity and offsets from the magic angle setting; for our systems $^{113}$Cd line widths of ca. 1 ppm (40 Hz) are usually obtained. The much larger line widths of approximately 400-500 Hz observed in the MAS spectra for both Cd-TPP and Py-Cd-TPP can be ascribed to the scalar $^{1}J(^{113}Cd-^{15}N)$ interactions which are not averaged out by magic angle spinning. Actually, spectral expansions of the individual spinning sidebands for Cd-TPP reveal the line shape of a broadened 1:4:6:4:1 quintet with $^{1}J(^{113}Cd-^{15}N) \approx 160 \pm 20$ Hz, i.e., a magnitude similar to the value $^{1}J(^{113}Cd-^{15}N) = 150.1$ Hz observed for Py-Cd-TPP in the liquid state.

(46) Reference 2, Chapter 8.
(47) B. Bak, D. Christensen, L. Hansen, and F. Rastrup-Anderson, *J. Chem. Phys.*, **24**, 720 (1956).
(48) T. Bundgaard, H. J. Jakobsen, and E. Rahkamaa, *J. Magn. Reson.*, **19**, 345 (1975).
(49) Reference 43, Chapter 4.
(50) T. Bundgaard and H. J. Jakobsen, *Tetrahedron Lett.*, 1621 (1976).
(51) Reference 33, p 78.
(52) U. Haeberlen, "High Resolution NMR in Solids", Supplement 1 in "Advances in Magnetic Resonance", Academic Press, New York, 1976.
(53) M. Mehring, "High Resolution NMR Spectroscopy in Solids", Springer-Verlag, New York, 1976.

(54) (a) The observed line shape for Cd-TPP is due to the dead time of our receiver. This can be circumvented by the use of spin echoes.[55] (b) The axial symmetry observed for Py-Cd-TPP indicates the pyridine ligand is executing rapid diffusion (or fourfold jumps) about its twofold axis.

Table II. $^{113}$Cd Chemical Shift Tensors[a] for Cd-TPP and Py-Cd-TPP

| | $\bar{\sigma}$[b] | $\sigma_\parallel$ | $\sigma_\perp$ | $\Delta\sigma$[c] |
|---|---|---|---|---|
| Cd-TPP[d] | −399 | −626 | −285 | −341 |
| Py-Cd-TPP[e] | −432 | −502 | −397 | −105 |

[a] All shifts are in ppm from external $Cd(ClO_4)_2 \cdot 6H_2O$; negative shifts to lower shielding, no bulk susceptibility corrections. [b] $\bar{\sigma} = (\sigma_\parallel + 2\sigma_\perp)/3$. [c] $\Delta\sigma = \sigma_\parallel - \sigma_\perp$. [d] Estimated errors, ±3 ppm. [e] Estimated errors, ±2 ppm.

Line shapes of NMR powder patterns are well understood and have been the subject of several reviews.[51-53] From the prominent features of these spectra, such as for those in Figure 8, it is often possible to derive the principal components of the shielding tensor ($\sigma_{xx}$, $\sigma_{yy}$, and $\sigma_{zz}$) directly. However, in most cases, the values derived in this way are used as starting parameters for a theoretical simulation of the experimental powder spectrum[51-53] in order to obtain more reliable parameters. We used another approach in that these parameters may also be determined from theoretical computer simulations of spinning sideband intensities for the MAS spectra observed at different spinning rates.[28,55,56] Figure 9 shows a series of such computer-simulated spinning spectra, generated from the theoretical treatment by Marciq and Waugh,[57] along with the corresponding experimental MAS spectra for Cd-TPP. However, a more direct procedure, which appears to be the method of choice, for obtaining the principal elements of the shielding tensor has recently appeared by Hertzfeld and Berger.[56] The $^{113}$Cd chemical shift tensor parameters extracted from the spectra of Cd-TPP and Py-Cd-TPP are tabulated in Table II.

The isotropic shift of 432 ppm observed for Py-Cd-TPP is similar to that observed from liquid-state NMR using $CDCl_3$ as solvent (Table I). Furthermore, the solid-state isotropic shift data in Table II shows that addition of pyridine as a fifth ligand to Cd-TPP shifts the $^{113}$Cd resonance to lower shielding by 33 ppm. The power of solid-state NMR spectroscopy is, however, best appreciated when it is realzied that this relatively small isotropic chemical shift difference is, in fact, the result of rather large changes in the individual shielding tensor elements moving in opposite directions. That is, the unique tensor element ($\sigma_\parallel$) for Py-Cd-TPP is shifted to higher shielding by 124 ± 5 ppm while the in-plane element ($\sigma_\perp$) is shifted to lower shielding by 112 ± 5 ppm relative to Cd-TPP. From these changes in the shift tensor elements, the structural factors that give rise to the observed isotropic chemical shift of 33 ppm may be argued qualitatively, i.e., an argument that would have been meaningless without the solid-state NMR information. If the pyridine (fifth) ligand is simply coordinating the in-plane cadmium of Cd-TPP via its $5p_z$ orbital (or an appropriate combination of cadmium orbitals) and without geometrical distortions, then large changes in the in-plane components of the $^{113}$Cd shielding tensor and only minor changes for the unique element are expected relative to Cd-TPP. However, if the fifth ligand pulls the cadmium out of the molecular plane, then gross changes are expected for all tensor elements. Obviously, from the data in Table II the latter situation prevails. This conclusion is consistent with the structural data available on five coordinate metalloporphyrins[2] and with a recent X-ray structure for the piperidine adduct of Cd-TPP.[58] It would be formally incorrect to conclude that nitrogen ligand binding to cadmium $5p_z$ orbital causes a shift of the unique tensor element to higher shielding. But rather, the observed shift for $\sigma_\parallel$ represents the combination of both ligand binding and the effect of the ligand moving out of the ring. A similar rationale exists for the in-plane element, $\sigma_\perp$.

This "orthogonal" interaction is expected if the "local paramagnetic" term is the dominant contributing mechanism to the observed shifts in the individual shielding tensor elements. This term is proportional to matrix elements of the following form[59]

$$\sigma_{zz} \alpha \left\langle \mu \left| \frac{L_z}{r^3} \right| \nu \right\rangle$$

where $\mu$ and $\nu$ are orbitals on the cadmium (for the sake of the present discussion $\mu$, $\nu$ and 5p orbitals) and $L_z$ is the $z$ component of angular momentum. From the symmetry of Py-Cd-TPP, the $5p_z$ orbital belongs to a different irreducible representation than the $5p_x$ and $5p_y$ orbitals. Hence, because of this symmetry constraint and the nature of the angular momentum operator, perturbations to the $5p_z$ orbital cannot directly contribute to $\sigma_{zz}$. Likewise, it is only perturbations to $5p_x$ and $5p_y$ that contribute $\sigma_{zz}$. Again, it must be recalled that such symmetry arguments assume the dominance of the one-center term. Clearly, more experimental data are needed to check such an assertion.

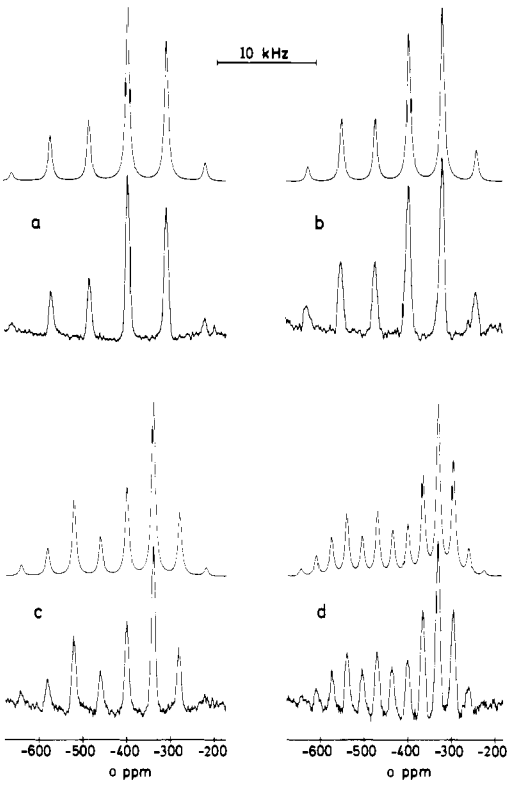


**Figure 9.** Experimental (lower) and simulated (upper) magic angle spinning (MAS) CP solid-state $^{113}$Cd NMR spectra of "free" Cd-TPP with spinning rates of (a) 3.396, (b) 3.417, (c) 2.685, and (d) 1.546 kHz. A value $\Delta\sigma = -341$ ppm has been used in the simulation of all theoretical MAS spectra.

Presently, our knowledge of Cd chemical shifts are based solely on experimental observations. One such observation is that a 100-ppm change in the Cd chemical shift can occur by seemingly trivial changes of the molecular system, for example, in going from $(CH_3)_2Cd$ to $(C_2H_5)_2Cd$[7c] or by substituting an oxygen for a nitrogen ligand.[9b,12,d] Hence, one has to exercise great caution in trying to interpret small chemical shift changes (less than 50 ppm) in terms of orbital polarization arguments which are valid for lighter elements (e.g., $^{13}$C). Until a general theoretical picture emerges for chemical shifts of heavier elements, one must rely upon a close emperical relationship between the benchmarks of solid-state chemical shift data and well-known structures. Here chemical shift means not only the isotropic chemical shift but also the elements of the Cd chemical shift tensor.

Our investigation on Py-Cd-TPP represents a special case of $^{113}$Cd solid-state NMR studies in general. The Cd chemical shift

(55) R. G. Griffin, G. Bodenhausen, R. A. Haberkorn, J. H. Haung, M. Munowitz, R. Osredkar, D. J. Ruben, R. E. Stark, and H. van Willigen, *Philos. Trans. R. Soc. London, Ser. A*, **299**, 547 (1981).
(56) J. Herzfeld and A. E. Berger, *J. Chem. Phys.*, **73**, 6021 (1980).
(57) M. Maricq and J. S. Waugh, *J. Chem. Phys.*, **70**, 3300 (1979).
(58) P. Rodesiler and E. L. Amma, unpublished results.
(59) R. Ditchfield and P. D. Ellis in "Topics in Carbon-13 NMR Spectroscopy", G. C. Levy, Ed., Wiley-Interscience, New York, 1974, p. 1.

Table III. Experimental $^{113}Cd$, $^{15}N$ and $^{13}C$ Spin-Lattice Relaxation Times, $T_1$, and Nuclear Overhauser Effects, $\eta$, along with Calculated Values for $\eta_{max}$, $T_1^{CSA}$, $T_1^{DD}$, and Rotational Correlation Times/Diffusion Constants for Py-Cd-TPP (1) and Py-$d_5$-Cd-TPP (1a)[a]

| nuclei | field, T | sample | $T_1$, s | $\eta$ | $\eta_{max}$ | $T_1^{CSA}$, s | $T_1^{DD}$, s |
|---|---|---|---|---|---|---|---|
| $^{113}Cd$ | 9.4 | 1/1a[b] | 10.30 ± 0.4 | −0.5 ± 0.04 | −2.07 ± 0.04 | 10.6 ± 0.6 | >225 |
| $^{113}Cd$ | 9.4 | 2[c] | 10.42 ± 0.20 | −0.06 ± 0.03 | −2.07 ± 0.04 | 10.75 ± 0.40 | 230-750 |
| $^{153}Cd$ | 4.7 | 1a | 28.5 ± 3.5 | −0.26 ± 0.04 | −2.19 ± 0.02 | 33.5 ± 7.0 | 135-620 |
| $^{15}N$ | 9.4 | 1a | 6.62 ± 0.10 | −0.05 ± 0.03 | −4.38 ± 0.11 | 6.70 ± 0.15 | >350 |
| $^{15}N$ | 2.3 | 1a | 95 ± 10 | −0.78 ± 0.03 | −4.89 ± 0.01 | 113 ± 13 | 510-690 |
| $^{15}N$ | 2.3 | 1 | 87 ± 6 | −0.91 ± 0.03 | −4.89 ± 0.01 | 107 ± 8 | 420-520 |
| $^{13}C\beta$ | 9.4 | 1a | 0.430 ± 0.010 | 1.82 ± 0.05 | 1.81 ± 0.03 | | 0.430 ± 0.010 |
| $^{13}C2$ | 9.4 | 1a | 0.627 ± 0.013 | | | | 0.627 ± 0.013 |
| $^{13}C3$ | 9.4 | 1a | 0.624 ± 0.015 | | | | 0.624 ± 0.015 |
| $^{13}C4$ | 9.4 | 1a | 0.434 ± 0.010 | | | | 0.434 ± 0.010 |

correlation times (s): $\tau_0 = (2.09 \pm 0.21) \times 10^{-10}$, $\tau_2 = (0.85 \pm 0.08) \times 10^{-10}$, $\tau^* = (5.2 \pm 1.9) \times 10^{-10}$
diffusion constants ($s^{-1}$): $D_\perp = (8.08 \pm 0.8) \times 10^8$, $D_\parallel = (2.56 \pm 0.32) \times 10^9$, $D^* = (2.2 \pm 0.8) \times 10^9$

[a] All relaxation times and rotational correlation times are in seconds. [b] These data are the average of four measurements (FIRFT, IRFT, and SR) for 1 and 1a. [c] Determined for the pyridine-$d_5$ adduct of $^{113}Cd$-[$^{14}N_4$]TPP (2).

tensor elements are axially symmetric and can be easily assigned to a molecule fixed coordinate system because of the molecular symmetry. Hence, one can envision a study with different axial ligands which would allow the separation of structural effects (i.e., the degree of nonplanarity of the cadmium with respect to the porphyrin ring) vs. electronic effects (e.g., ligand polarization of metal orbitals perpendicular/parallel to the ring plane). In general, the Cd chemical shift tensors do not have axial symmetry and therefore the only way that a Cd chemical shift tensor element can be assigned relative to a molecule fixed coordinate system is via the analysis of Cd shift tensors for selected single crystals. Work in this area is presently in progress in our laboratories.

**$^{113}Cd$, $^{15}N$, and $^{13}C$ Spin-Lattice Relaxation Data and Anisotropic Motion for Py-Cd-TPP.** The $^{113}Cd$, $^{15}N$, and $^{13}C$ spin-lattice relaxation parameters ($T_1$'s and NOE's) determined at different magnetic field strengths for the pyridine and/or pyridine-$d_5$ complex Py-Cd-TPP are summarized in Table III. This table also contains the spin-lattice relaxation data for the different mechanisms governing the relaxation of these nuclei along with the corresponding rotational correlation times/diffusion constants evaluated from these data based on the appropriate equations derived in the Theory section. The $T_1$ relaxation data and mechanisms for the individual nuclei are discussed separately below.

**$^{113}Cd$ Spin-Lattice Relaxation.** The effect of broad-band $^1H$ decoupling on the $^{113}Cd$ NMR spectrum of Py-Cd-TPP (**1**) at 9.4 T has been shown in Figure 4. Comparison of the spectral intensities for the $^1H$-decoupled spectra obtained with continuous and gated $^1H$ decoupling shows that the $^{113}Cd$-{$^1H$} NOE is very small ($\eta = -0.05$). Furthermore, the NOE's determined by using pyridine and pyridine-$d_5$ are identical within the experimental error at this field. Therefore, continuous $^1H$ decoupling has been employed for all $T_1(^{113}Cd)$ measurements. A total of four $T_1(^{113}Cd)$ measurements were performed for Py-Cd-TPP (**1**) using the methods of IRFT, FIRFT and SR via CRAPS. An average value of $T_1(^{113}Cd) = 10.3 \pm 0.4$ s has been determined from these measurements. Another value of $T_1(^{113}Cd) = 10.42 \pm 0.20$ s, determined from an IRFT measurement (14 $\pi$ values) of the single-line $^{113}Cd$ spectrum of Py-Cd-TPP possessing $^{14}N/^{15}N$ isotopically normal pyrrole nitrogens, is in excellent agreement with the average value obtained for **1**. The effect on $T_1(^{113}Cd)$ of changing the fifth ligand from pyridine to pyridine-$d_5$ for **1** is within the experimental error of the measurements. Examination of $T_1(^{113}Cd)$ and $^{113}Cd$-{$^1H$} NOE at a magnetic field of 4.7 T reveals increases for the magnitudes of $T_1(^{113}Cd)$ as well as the NOE. Because of the extremely long spectrometer time required for these experiments at the lower field (reduced sensitivity and longer spin-lattice relaxation time), only a single determination was performed and with reduced accuracy (eight $\tau$ values and lower S/N ratio) as compared to the 9.4-T data. However, the $T_1(^{113}Cd)$ value of approximately 30 s and $\eta = -0.26$ at 4.7 T show that $^{113}Cd$ spin-lattice relaxation at 9.4 T is dominated by the mechanism of chemical shift anisotropy (CSA). Furthermore, $^{113}Cd$-$^1H$ dipole-dipole relaxation (interaction with the porphyrin-ring pyrrole and/or phenyl protons) becomes increasingly important at lower magnetic field strengths, although it is rather inefficient.

The extraction of meaningful values for the contributions of these mechanisms to the $^{113}Cd$ spin-lattice relaxation was performed by using the more precise experimental data obtained at 9.4 T only and the relationships

$$(T_{1,obsd})^{-1} = (T_1^{CSA})^{-1} + (T_1^{DD})^{-1} \quad (36)$$

$$T_1^{DD} = (\eta_{max}/\eta_{obsd})T_{1,obsd} \quad (37)$$

which may be combined to give

$$T_1^{CSA} = \frac{\eta_{max}}{\eta_{max} - \eta_{obsd}} T_{1,obsd} \quad (38)$$

As pointed out elsewhere,[8] the value for $\eta_{max}$ may not be equal to −2.25 ($\eta_{max}$ for the extreme narrowing condition) at a field of 9.4 T. Therefore, the value for $\eta_{max}$ to be used in eq 37 and 38 has been derived from iterative numerical calculations based on the appropriate equations in the Theory section (eq 8-13, 15, and 27) and the experimental relaxation data for $^{113}Cd$ and $^{13}C$ (vide infra) along with the value for $|\Delta\sigma|$ (=105 ppm) from $^{113}Cd$ solid-state NMR.[60] Values of −2.07 and −2.19 were obtained for $\eta_{max}$ at 9.4 and 4.7 T, respectively. The resulting value of 10.6 s for $T_1^{CSA}(^{113}Cd)$ at 9.4 T agrees within the experimental errors with the relaxation data determined at 4.7 T (Table III).

**$^{15}N$ Spin-Lattice Relaxation.** The $^{15}N$ spin-lattice relaxation behavior observed for the pyrrole nitrogen atoms of Py-Cd-TPP (**1**) parallels the $^{113}Cd$ nucleus. A precise value for $T_1(^{15}N)$ (=6.62 ± 0.10 s) at 9.4 T has been determined from IRFT experiments (18 $\tau$ values) using continuous $^1H$ decoupling. The $^{15}N$-{$^1H$} NOE's at 9.4 T, using either pyridine or pyridine-$d_5$ as the fifth ligand, are extremely small, although slightly different. At the lower magnetic field of 2.3 T, the difference in NOE's, using pyridine and pyridine-$d_5$ as a ligand, becomes more pronounced (Table III) as the NOE approaches the value $\eta = -1$ which would give rise to signal cancellation under condition of continuous $^1H$ decoupling. This shows that, although the pyridine ligand exchange is fast on the chemical shift ($^{13}C$) time scale, the pyridine (H$\alpha$) protons make a small contribution to the $^{15}N$-$^1H$ dipole-dipole part of the $^{15}N$ relaxation. However, even at the low field of 2.3 T, the total contribution from the D-D mechanism constitutes only ca. 18% of the total $^{15}N$ relaxation rate for the

(60) The calculations of $\eta_{max}$ for the $^{113}Cd$-{$^1H$} and $^{15}N$-{$^1H$} NOE's using eq 27 were performed only for an in-plane proton, i.e., the H$\beta$ "pyrrole" proton. The additional correlation time for the phenyl-group protons, because of the internal motion of this group, greatly complicates the calculation of $\eta_{max}$ for, e.g., the ortho phenyl protons. Although this may give different $\eta_{max}$ values for these protons, the errors introduced in the calculation of $T_1^{CSA}$ from eq 36-38 are estimated to be negligible because of the very small experimental values, $\eta_{obsd}$, for $^{113}Cd$ and $^{15}N$ at 9.4 T and because the effect of the anisotropic motion on $\eta_{max}$ is almost insignificant at the lower magnetic fields. An experimental determination of the NOE contribution from the phenyl-group protons will be investigated by using Py-$d_5$-Cd-TPP possessing perdeuterated phenyl groups.

mechanisms governing the $^{15}N$ spin–lattice relaxation. From the observed field dependence of the relaxation data at 9.4 and 2.3 T (i.e., $T_1(^{15}N)$ = 6.62 ± 0.10 s and $T_1(^{15}N)$ = 95 ± 10 s, respectively) we conclude that $T_1(^{15}N)$ at either field can be accounted for by the mechanisms of CSA and $^{15}N$–$^1H$ DD relaxation only. Furthermore, the $^{15}N$ spin–lattice relaxation at 9.4 T is almost completely governed by the CSA mechanism. The contributions from these mechanisms at 9.4 and 2.3 T, calculated from eq 36 and 37, are given in Table III. The values for $\eta_{max}$, −4.38, and −4.89 at 9.4 and 2.3 T, respectively, applied in eq 37 and 38 were calculated from eq 27 by using the diffusion constants determined from the $^{113}Cd$ and $^{13}C$ relaxation data (vide infra).[60]

From the value obtained at 9.4 T for $T_1^{CSA}(^{15}N)$ (=6.70 ± 0.15), we have estimated the $^{15}N$ chemical shift anisotropy, $\Delta\sigma$, to be within the range $|\Delta\sigma|$ = 279 ± 12 ppm using eq 14, the $\tau_2$ and $\tau_0$ values (Table III) obtained from the $^{113}Cd$ and $^{13}C$ relaxation data (vide infra), and finally the full range for the asymmetry parameter $\eta$ ($0 \le \eta \le 1$). The upper limit for $|\Delta\sigma|$ (=291 ppm) corresponds to $\eta = 0$ while $|\Delta\sigma|$ = 267 ppm is obtained for $\eta = 1$.

Approximate values for the $^{15}N$–{$^1H$} NOE ($\eta \approx 0$) and $T_1(^{15}N)$ (~56 s) have been reported earlier for the related zinc porphyrin, Zn–[$^{15}N_4$]TPP,[15d,42] at 18.25 MHz (4.2 T). The relaxation results reported in the present work show that $^{15}N$ NMR studies of metalloporphyrin derivatives are preferably performed at high magnetic fields (~10 T). The failure to directly observe the $^{15}N$ resonances for $^{15}N$-enriched chlorophyll *a*[15a] and hemoglobin[15b] is most likely caused by the unfavorable relaxation data ($T_1$ and NOE) at lower magnetic fields.

**$^{13}C$ Spin–Lattice Relaxation.** Accurate values for the $^{13}C$ spin–lattice relaxation times have been measured at 9.4 T (100.62 MHz) for all protonated carbons in Py–Cd–TPP (**1**). The experimental results are given in Table III. The $^{13}C$ relaxation for these carbons are all completely governed by the $^{13}C$–$^1H$ dipole–dipole mechanism as reflected by the $^{13}C$–{$^1H$} NOE's which approach the limiting value for $\eta_{max}$ (=1.99) (observed under conditions of extreme narrowing and isotropic motion). Extreme care has been exercised in the determination of a precise value for the $^{13}C\beta$ NOE, $\eta$ = 1.82 ± 0.05. Since this value, as well as $T_1^{DD}(^{13}C\beta)$, at least at 9.4 T, is expected to reflect the anisotropic motion ($\rho = D_\parallel/D_\perp$) according to the eq 8–12, 15, and 27. All $^{13}C$ relaxation data were analyzed in terms of the anisotropic motion ($\rho$) for the Py–Cd–TPP moiety and/or the internal librational motion of the phenyl groups. Details are given in the following section.

**Anisotropic Motions for Py–Cd–TPP.** Two kinds of anisotropic motion for the Py–Cd–TPP complex in solution have been examined. First, the anisotropic diffusion, $\rho = D_\parallel/D_\perp$, for the complex as a whole has been analyzed in terms of the equations derived in the Theory section and using the experimental $^{113}Cd$ and $^{13}C$ liquid-state relaxation data and $^{113}Cd$ CSA, $\Delta\sigma$ = 105 ± 2 ppm, determined from solid-state NMR. Second, the anisotropic librational motion executed by the phenyl-group substituents, on a molecular frame which itself is undergoing anistotropic rotational diffusion, may be determined from eq 19–25 by using the phenyl-carbon $^{13}C2$ (or $^{1o}C3$) dipolar relaxation rate and the values derived for $D_\parallel$ and $D_\perp$.

The $^{113}Cd$ CSA relaxation in Py–Cd–TPP is given by eq 13 which shows that $T_1^{CSA}$ ($^{113}Cd$) is independent of $\rho$ and only depends on $\tau_0 = (6D_\perp)^{-1}$. Thus, using the experimental data determined at 9.4 T, i.e., $T_1^{CSA}(^{113}Cd)$ = 10.6 ± 0.6 s, and $\Delta\sigma$ = 105 ± 2 ppm, a value for $\tau_0$ = (2.09 ± 0.21) × $10^{-10}$ s ($D_\perp$ = (8.08 ± 0.80) × $10^8$ $s^{-1}$) is obtained. The $^{13}C$–$^1H$ dipolar relaxation for the pyrrole C$\beta$ carbon is given by eq 8, 10, 12, and 15 and thus is a function of both $\tau_0$ and $\tau_2$. With the above value of $D_\perp$, determined by the $^{113}Cd$ CSA relaxation, and $T_1^{DD}(^{13}C\beta)$ = 0.43 ± 0.01 s, one can extract a value for $D_\parallel$ = (2.56 ± 0.32) × $10^9$ $s^{-1}$. Therefore, the anisotropy in the motion for Py–Cd–TPP is $\rho = D_\parallel/D_\perp$ = 3.2 ± 0.8. In these and other calculations of $^{13}C$–$^1H$ dipolar relaxation rates (eq 8), we assume a value $r$ = 1.08 Å for the one-bond $^{13}C$–$^1H$ distance. From the diffusion constants $D_\parallel$ and $D_\perp$, a value has been calculated for the maximum NOE of the pyrrole C$\beta$ carbon, $\eta_{max}^{calcd}$ = 1.81 ± 0.03. This value is similar to that determined experimentally, $\eta_{obsd}$ = 1.82 ± 0.05. It is noteworthy that on the basis of the $^{13}C$ relaxation data ($T_1^{DD}$ and NOE) at 9.4 T *alone*, it is possible to obtain an estimate of the anisotropic rotational diffusion for Py–Cd–TPP within reasonable error limits. Thus, using the $^{13}C\beta$ relaxation data determined at 9.4 T and using eq 8, 10, 12, 15, and 27, one can calculate $\rho$ to be within the range of $1.5 < \rho < 4.5$. Obviously, a more precise value for the anisotropic motion is obtained from a combination of $^{113}Cd$ CSA and $T_1^{DD}(^{13}C\beta)$ relaxation data.

The anisotropic librational motion of the phenyl-group substituents in Py–Cd–TPP has been calculated from eq 8 and 19–25 by using the $^{13}C$–$^1H$ dipolar relaxation rates determined for the C2 (ortho) and C3 (meta) phenyl carbons (i.e., $T_1^{DD}(C2) = T_1^{DD}(C_3)$ = 0.625 ± 0.015 s) and the diffusion constants $D_\parallel$ and $D_\perp$ determined for the anisotropic motion of the complex. As shown in the Theory section, identical relaxation rates are obtained for $\theta = \pi/3$ and $\theta = 2\pi/3$ in accordance with the experimental results for C3 and C2, respectively. A value $D^*$ = (2.2 ± 0.8) × $10^9$ $s^{-1}$ ($\tau^*$ = (5.2 ± 1.9) × $10^{-10}$ s) is determined for the diffusion constant describing the rotational motion of the phenyl-ring substituents around the C1–C4 axis relative to the porphyrin-ring skeleton. Finally, the $^{13}C$–$^1H$ dipolar relaxation time for the C4 (para) phenyl carbon, $T_1^{DD}$ = 0.43 ± 0.01 s, is identical with that observed for the pyrrole C$\beta$ carbon. This is in accordance with the expression for $J(\omega)$ in eq 19 since, for this case, the C–H vector lies along the internal rotational diffusion axis ($\theta = 0°$). Thus, the expression for $J(\omega)$ reduces to eq 9, and hence the relaxation for the C4–H4 vector is independent of the internal motion of the phenyl group.

## Conclusion

The $^{113}Cd$, $^{15}N$, and $^{13}C$ chemical shifts, along with the signs and magnitudes of the various spin–spin coupling constants between these nuclei, have been determined for the pyridine adduct of $^{113}Cd$ and $^{15}N$ multiply labeled cadmium *meso*-tetraphenylporphyrin, Py–Cd–TPP. Further, the spin–lattice relaxation times for these nuclides have been determined in conjunction with their respective mechanisms at three magnetic fields (2.3, 4.7, and 9.4 T). It has been found useful to employ solid-state $^{113}Cd$ NMR experiments (both static and with magic angle spinning) to completely analyze the field-dependent relaxation data. These data have been discussed and analyzed in terms of the motion of the Cd–TPP frame which is undergoing anisotropic diffusion with an axially symmetric diffusion tensor. The anisotropy in the motion, $D_\parallel/D_\perp$, is found to be 3.2 ± 0.8.

Magic angle spinning experiments afforded the determination that the $^{113}Cd$ chemical shift of Py–Cd–TPP was 33 ppm to lowering shielding than that of "unliganded" Cd–TPP. With the aid of the static powder spectra, this chemical shift difference may be accounted for in terms of the pyridine donor properties and the ability of this ligand to pull the cadmium out of the molecular plane.

Finally, it is evident that NMR investigations involving less receptive nuclei, such as $^{15}N$, $^{113}Cd$, $^{195}Pt$, $^{103}Rh$, etc., can be made much easier if they are performed at high magnetic fields (7 T or higher) owing to the relative importance of the chemical shift anisotropy relaxation mechanism at the higher fields.

**Acknowledgment.** We acknowledge the NATO Science Affairs Division, Brussels (Research Grant No. 1831), the Danish Natural Science Research Council (J. No. 11-2147), and the National Institute of Health (GM 26295) for partial support of this research. The use of the facilities at the University of South Carolina NMR Center, funded by the National Science Foundation (CHE 78-18723), is acknowledged. Finally, we thank Mr. Karl E. Holst for synthesizing $^{113}Cd$-[$^{15}N_4$]TPP.

**Registry No.** Cd-TPP, 14977-07-2; $^{113}Cd$[$^{15}N_4$]TPP, 83632-68-2; [$^{15}N_4$]$H_2$TPP, 71771-09-0; $^{113}Cd(OCOCH_3)_2$, 83615-91-2; [$^{15}N$]-Py$^{113}Cd$[$^{15}N_4$]TPP, 83632-69-3; $^{113}Cd$, 14336-66-4.